and Welfare. We are grateful to M. Yokoe, M. Terada, N. Takahira, and M. Sudo for their excellent technical assistance. Rat strain F344-*Hr*^{krh} (NBRP Rat No: 0471) is deposited in the National BioResource Project-Rat.

References

1. Ahearn, K., Akkouris, G., Berry, P.R., Chrissluis, R.R., Crooks, I.M., Dull, A.K., Grable, S., Jeruzal, J., Lanza, J., Lavoie, C., Maloney, R.A., Pitruzzello, M., Sharma, R., Stoklasek, T.A., Tweeddale, J., and King, T.R. 2002. The Charles River "hairless" rat mutation maps to chromosome 1: allelic with fuzzy and a likely orthologue of mouse frizzy. *J. Hered.* 93: 210–213.
2. Ahmad, W., Faiyaz ul Haque, M., Brancolini, V., Tsou, H.C., ul Haque, S., Lam, H., Aita, V.M., Owen, J., deBlaquiere, M., Frank, J., Cserhalmi-Friedman, P.B., Leask, A., McGrath, J.A., Peacocke, M., Ahmad, M., Ott, J., and Christiano, A.M. 1998. Alopecia universalis associated with a mutation in the human hairless gene. *Science* 279: 720–724.
3. Ahmad, W., Ratterree, M.S., Panteleyev, A.A., Aita, V.M., Sundberg, J.P., and Christiano, A.M. 2002. Atrichia with papular lesions resulting from mutations in the rhesus macaque (*Macaca mulatta*) hairless gene. *Lab. Anim.* 36: 61–67.
4. Ahmad, W., Zlotogorski, A., Panteleyev, A.A., Lam, H., Ahmad, M., ul Haque, M.F., Abdallah, H.M., Dragan, L., and Christiano, A.M. 1999. Genomic organization of the human hairless gene (*HR*) and identification of a mutation underlying congenital atrichia in an Arab Palestinian family. *Genomics* 56: 141–148.
5. Aitman, T.J., Critser, J.K., Cuppen, E., Dominiczak, A., Fernandez-Suarez, X.M., Flint, J., Gauguier, D., Geurts, A.M., Gould, M., Harris, P.C., Holmdahl, R., Hubner, N., Izsvak, Z., Jacob, H.J., Kuramoto, T., Kwitek, A.E., Marrone, A., Mashimo, T., Moreno, C., Mullins, J., Mullins, L., Olsson, T., Pravenec, M., Riley, L., Saar, K., Serikawa, T., Shull, J.D., Szpirer, C., Twigger, S.N., Voigt, B., and Worley, K. 2008. Progress and prospects in rat genetics: a community view. *Nat. Genet.* 40: 516–522.
6. Bazzi, H., Kljuic, A., Christiano, A.M., and Panteleyev, A.A. 2004. Intragenic deletion in the Desmoglein 4 gene underlies the skin phenotype in the Iffa Credo "hairless" rat. *Differentiation* 72: 450–464.
7. Bult, C.J., Eppig, J.T., Kadin, J.A., Richardson, J.E., and Blake, J.A. 2008. The Mouse Genome Database (MGD): mouse biology and model systems. *Nucleic Acids Res.* 36: D724–728.
8. Cachon-Gonzalez, M.B., San-Jose, I., Cano, A., Vega, J.A., Garcia, N., Freeman, T., Schimmang, T., and Stoye, J.P. 1999. The hairless gene of the mouse: relationship of phenotypic effects with expression profile and genotype. *Dev. Dyn.* 216: 113–126.
9. Cichon, S., Anker, M., Vogt, I.R., Rohleder, H., Putzstuck, M., Hillmer, A., Farooq, S.A., Al-Dhafri, K.S., Ahmad, M., Haque, S., Rietschel, M., Propping, P., Kruse, R., and Nothen, M.M. 1998. Cloning, genomic organization, alternative transcripts and mutational analysis of the gene responsible for autosomal recessive universal congenital alopecia. *Hum. Mol. Genet.* 7: 1671–1679.
10. Dagati, V. 1994. The many masks of focal segmental glomerulosclerosis. *Kid. Int.* 46: 1223–1241.
11. Friedman, J.M., Leibel, R.L., and Bahary, N. 1991. Molecular mapping of obesity genes. *Mamm. Genome* 1: 130–144.
12. Inazu, M. and Sakaguchi, T. 1984. Morphologic characteristics of the skin of bald mutant rats. *Lab. Anim. Sci.* 34: 584–587.
13. Ishii, Y., Tsutsui, S., Doi, K., and Itagaki, S. 1997. Hair follicles of young Wistar strain hairless rats: a histological study. *J. Anat.* 191: 99–106.
14. Kawaji, H., Tsukuda, R., and Nakaguchi, T. 1980. Immunopathology of rhino mouse, an autosomal recessive mutant with murine lupus-like disease. *Acta Pathol. Jpn.* 30: 515–530.
15. Kuramoto, T., Kitada, K., Inui, T., Sasaki, Y., Ito, K., Hase, T., Kawagachi, S., Ogawa, Y., Nakao, K., Barsh, G.S., Nagao, M., Ushijima, T., and Serikawa, T. 2001. Attractin/mahogany/zitter plays a critical role in myelination of the central nervous system. *Proc. Natl. Acad. Sci. U.S.A.* 98: 559–564.
16. Mashimo, T., Yanagihara, K., Tokuda, S., Voigt, B., Takizawa, A., Nakajima, R., Kato, M., Hirabayashi, M., Kuramoto, T., and Serikawa, T. 2008. An ENU-induced mutant archive for gene targeting in rats. *Nat. Genet.* 40: 514–515.
17. Nanashima, N., Akita, M., Yamada, T., Shimizu, T., Nakano, H., Fan, Y., and Tsuchida, S. 2008. The hairless phenotype of the Hirosaki hairless rat is due to the deletion of an 80-kb genomic DNA containing five basic keratin genes. *J. Biol. Chem.* 283: 16868–16875.
18. Nose, M. 2007. A proposal concept of a polygene network in systemic vasculitis: lessons from MRL mouse models. *Allergol. Int.* 56: 79–86.
19. Nose, M., Nishimura, M., and Kyogoku, M. 1989. Analysis of granulomatous arteritis in MRL/Mp autoimmune disease mice bearing lymphoproliferative genes. The use of mouse genetics to dissociate the development of arteritis and glomerulonephritis. *Am. J. Pathol.* 135: 271–280.
20. Panteleyev, A.A., Botchkareva, N.V., Sundberg, J.P., Christiano, A.M., and Paus, R. 1999. The role of the hairless (*hr*) gene in the regulation of hair follicle catagen transformation. *Am. J. Pathol.* 155: 159–171.
21. Serikawa, T., Mashimo, T., Takizawa, A., Okajima, R., Maedomari, N., Kumafuji, K., Takami, F., Neoda, Y., Otsuki, M., Nakanishi, S., Yamasaki, K., Voigt, B., and Kuramoto, T. 2009. National BioResource Project-Rat and related activities. *Exp. Anim.* 58: 333–341.
22. Sun, J., Silva, K.A., McElwee, K.J., King, L.E., and Sundberg, J.P. 2008. The C3H/HeJ mouse and DEBR rat models for alopecia areata: review of preclinical drug screening approaches and results. *Exp. Dermatol.* 17: 793–805.
23. Thompson, C.C., Sisk, J.M., and Beaudoin, G.M. 3rd. 2006. Hairless and Wnt signaling: allies in epithelial stem cell differentiation. *Cell Cycle* 5: 1913–1917.

OPEN ACCESS Freely available online PLOS GENETICS

A Mutation in the Gene Encoding Mitochondrial Mg^{2+} Channel MRS2 Results in Demyelination in the Rat

Takashi Kuramoto[1]*, Mitsuru Kuwamura[2], Satoko Tokuda[1,2], Takeshi Izawa[2], Yoshifumi Nakane[1], Kazuhiro Kitada[1,3], Masaharu Akao[4], Jean-Louis Guénet[5], Tadao Serikawa[1]

1 Institute of Laboratory Animals, Graduate School of Medicine, Kyoto University, Kyoto, Japan, **2** Laboratory of Veterinary Pathology, Osaka Prefecture University, Osaka, Japan, **3** Laboratory of Mammalian Genetics, Genome Dynamics Research Center, Graduate School of Science, Hokkaido University, Sapporo, Japan, **4** Department of Cardiovascular Medicine, Graduate School of Medicine, Kyoto University, Kyoto, Japan, **5** Département de Biologie du Développement, Institut Pasteur, Paris, France

Abstract

The rat demyelination (*dmy*) mutation serves as a unique model system to investigate the maintenance of myelin, because it provokes severe myelin breakdown in the central nervous system (CNS) after normal postnatal completion of myelination. Here, we report the molecular characterization of this mutation and discuss the possible pathomechanisms underlying demyelination. By positional cloning, we found that a G-to-A transition, 177 bp downstream of exon 3 of the *Mrs2* (MRS2 magnesium homeostasis factor (*Saccharomyces cerevisiae*)) gene, generated a novel splice acceptor site which resulted in functional inactivation of the mutant allele. Transgenic rescue with wild-type *Mrs2*-cDNA validated our findings. *Mrs2* encodes an essential component of the major Mg^{2+} influx system in mitochondria of yeast as well as human cells. We showed that the *dmy/dmy* rats have major mitochondrial deficits with a markedly elevated lactic acid concentration in the cerebrospinal fluid, a 60% reduction in ATP, and increased numbers of mitochondria in the swollen cytoplasm of oligodendrocytes. MRS2-GFP recombinant BAC transgenic rats showed that MRS2 was dominantly expressed in neurons rather than oligodendrocytes and was ultrastructurally observed in the inner membrane of mitochondria. Our observations led to the conclusion that *dmy/dmy* rats suffer from a mitochondrial disease and that the maintenance of myelin has a different mechanism from its initial production. They also established that Mg^{2+} homeostasis in CNS mitochondria is essential for the maintenance of myelin.

Citation: Kuramoto T, Kuwamura M, Tokuda S, Izawa T, Nakane Y, et al. (2011) A Mutation in the Gene Encoding Mitochondrial Mg^{2+} Channel MRS2 Results in Demyelination in the Rat. PLoS Genet 7(1): e1001262. doi:10.1371/journal.pgen.1001262

Editor: Gregory S. Barsh, Stanford University, United States of America

Received June 5, 2010; **Accepted** November 29, 2010; **Published** January 6, 2011

Funding: This work was supported by grants-in-aid for Scientific Research from the Japan Society for the Promotion of Science [21300153 to TK] and a grant-in-aid for Cancer Research from the Ministry of Health, Labour, and Welfare. The funders had no role in study design, data collection and analysis, decision to publish, or preparation of the manuscript.

Competing Interests: The authors have declared that no competing interests exist.

* E-mail: tkuramot@anim.med.kyoto-u.ac.jp

Introduction

Myelin is an essential component of the nervous tissue of higher vertebrates. It acts as a natural insulator of axonal segments allowing, at the same time, the maintenance of axonal integrity and the fast conduction of action potentials. It also reduces ionic currents across the axonal membrane and stabilizes the extracellular milieu within rapidly-firing axon bundles.

In the central nervous system (CNS), myelin is produced by oligodendrocytes, while in the peripheral nervous system (PNS), this function is achieved by Schwann cells. Myelination is completed within a relatively short period of time during mammalian development and requires a high rate of production and transport of different kinds of molecules, mostly proteins and lipids. In adult life, myelin is constantly remodeled and the maintenance of functional myelin sheaths requires a careful balance of *de novo* synthesis and turnover. It is quite clear that any event generating an imbalance in the myelination or remyelination process has the greatest chance of inducing dys- or demyelination of either the central or peripheral nervous system.

Our knowledge of the myelination process has benefited from careful observations conducted on human patients affected by one of the many defects of myelination or myelin turnover. It has also benefited from researches carried out on animal models, mostly mutant mice and rats, including those that have been induced by transgenesis or genetic engineering in ES cell lines [1,2]. Some of these models have even allowed therapies to be developed in a preclinical setting [3]. Unfortunately, only a small number of the many genes that are directly or indirectly involved in the myelination process have been identified and only a few of these genes have been functionally annotated, for example, by the characterization of one or more mutant alleles. For this reason, any new mutation occurring spontaneously or after mutagenesis is of potential interest for unraveling the molecular mechanisms involved in myelin assembly.

In an earlier paper we reported the discovery and pathology of a rat mutation designated *demyelination* (symbol *dmy*), which is characterized by severe and progressive myelin breakdown in the CNS. We mapped the locus responsible for this myelin disorder to rat chromosome (Chr) 17, very close to the prolactin (*Prl*) locus, in a region homologous to human Chr 6p21.1-22.3 and mouse Chr 13 [4,5]. Based on its pathological features, as well as its genetic localization, this demyelination syndrome appeared to be unique, with no homologue so far reported in any other mammalian species, including humans.

Author Summary

The myelin sheath that surrounds the axon of a neuron acts as a biological insulator. Its major function is to increase the speed at which impulses propagate along myelinated fibers in the central nervous system, as well as the peripheral nervous system. Alterations or damage affecting this structure (demyelination) result in the disruption of signals between the brain and other parts of the body. In the rat, mutations producing demyelination have been frequently identified and characterized and have contributed to a better understanding of the genetics of myelin development, physiology, and pathology. This paper reports the molecular characterization of a recessive allele responsible for the progressive disruption of myelin that was initially observed in mutant rats, previously named demyelination (*dmy*). This mutation generates an additional splicing acceptor site in an intron of the mitochondrial Mg^{2+} transporter gene (*Mrs2*), resulting in the insertion of a 83-bp genomic DNA segment into the *Mrs2* transcript and complete functional inactivation of the mutant allele. We firstly defined the biological function of MRS2 in mammals and demonstrated the crucial and unexpected role of MRS2 in myelin physiology. Our findings might be helpful in the development of new therapeutic strategies for demyelinating syndromes.

In this report we demonstrate that the causative gene (*Mrs2*) encodes a protein that is an essential component of the major electrophoretic Mg^{2+} influx system in mitochondria [6]. This gene has orthologues in other organisms, including lower eukaryotes and plants [7,8]. The protein shares many of the properties of bacterial CorA and yeast Alr1 proteins but its specific involvement in the myelination process was not known or even suspected.

Results

dmy/dmy rats exhibit a phenotype with typical demyelination

The pathology of homozygous *dmy/dmy* rats has been reported in detail previously [4]. Mutant rats exhibit no significant differences from their control littermates until 4 weeks of age. From 5 weeks on, flaccidity of the hind limbs becomes noticeable and evolves towards complete paralysis around 7–8 weeks of age. Progressive demyelination is observed in several parts of the CNS (Figure 1), namely the corpus callosum, the capsula interna, the striatum and the cerebellar peduncle, with major effects on the ventral and lateral parts of the spinal cord. Astrogliosis, which is a major feature of myelin disorder, is observed in demyelinated areas but motor neurons remain normal and there is no sign of associated inflammation in the white matter. The *dmy* mutation can then be regarded as a mutation affecting the maintenance and turnover of myelin rather than its initial production: this is typical demyelination [9].

The *dmy* syndrome is associated with a mutation in a splicing site of *Mrs2*, a gene encoding a mitochondrial Mg^{2+} channel

Out of 687 *dmy/dmy* mutant rats, collected from the 3,252 offspring of an intercross segregating for the *dmy* mutation, 23 individuals were found to carry a recombinant haplotype between the two loci that were used for the initial genetic mapping, namely; *Prl* (prolactin) and *Hh1ts* (testis-specific histone, H1t). Further investigation of these animals, using three novel informative SSLP markers, allowed us to narrow the genetic interval containing *dmy* down to 0.22 cM, between markers *D17Kur17* and *D17Got45*. Within this critical section, we found no recombination between the *dmy* locus and either *Aldh5a1* (aldhehyde dehydrogenase family 5, subfamily A1) or *Mrs2* (mitochondrial 118 RNA splicing2) loci, among $687 \times 2 = 1{,}374$ meioses. The rat genome databases revealed that *D17Kur17* and *D17Got45* were at position 46.78-Mb and 47.26-Mb, respectively, on rat Chr 17, yielding a physical size of 0.48 Mb of DNA for the interval containing the *dmy* locus. This stretch of DNA contained 6 genes (Figure 2A).

Analysis by RT-PCR of the transcription products of these 6 genes revealed that the cDNA transcribed from the *Mrs2* gene was larger in *dmy/dmy* mutants than in the controls (Figure 2B). After sequencing, we found that the larger size of the *dmy* cDNA was due to the insertion of an 83 bp intronic sequence between exons 3 and 4. Comparison of the two genomic sequences revealed a G-to-A transition, 177 bp downstream of the end of exon 3 (Figure 2C, Figure S1), generating a novel splice acceptor site, which accounted for the addition of the 83bp stretch of intronic sequence to the mutant transcript. In addition, while the *Mrs2* gene normally encodes a 434 amino-acid protein, the intronic insertion leads to a shorter protein (106 amino acids) due to the occurrence of a stop codon as a consequence of frame shifting within the novel pseudo-exon X. The new protein consisted of the first 91 amino acids of normal (wild-type) MRS2 protein followed by an additional 15 amino acids transcribed from the intronic stretch (Figure 2D) [10]. No nucleotide alteration was observed between normal and mutant haplotypes in the cDNA transcribed from the other 5 genes (*Vmp*, *Dcdc2*, *Gpld1*, *Aldh5a1*, and *KIAA0319*). These findings strongly suggested that the G-to-A mutation in intron 3 of *Mrs2* in *dmy/dmy* rats was very likely causative of the neurological phenotype.

dmy/dmy rats exhibit morphological and biochemical features characteristic of mitochondrial deficiencies

The MRS2 protein functions as a major transporter protein (Mg^{2+}, Ni^{2+} and Co^{2+}) in yeast as well as in human cells [10,11]. When this protein is functionally defective this leads to the "petite" phenotype in yeast and to cell death in human HEK 293 cells [11,12]. Because mitochondrial diseases in mammals are often accompanied by elevated lactic acid, reduced ATP, increased cytochrome oxidase (COX) activity, and the morphological alteration of mitochondria [13–15], we measured lactic acid levels and ATP contents in the CNS and performed morphological analyses of the CNS of *dmy/dmy* rats.

Lactic acid concentration in the cerebrospinal fluids was significantly elevated in *dmy/dmy* rats when compared with normal littermates: 126 ± 43.7 mg/dL vs 25 ± 9.6 mg/dL (average $\pm$ SD), $P<0.002$ (Figure 3A). The ATP concentration was markedly reduced in *dmy/dmy* rats: 265 ± 79 μM/mg vs 99 ± 46 μM/mg (average $\pm$ SD), $P<0.005$ (Figure 3B). In the affected *dmy/dmy* rats, swollen oligodendrocytes were often observed in the white matter, showing the increased COX reaction products (Figure 3C). Ultrastructurally, their cytoplasm contained many mitochondria and Golgi apparatus-like membrane structures (Figure 3D). These findings indicated that the mitochondria of *dmy/dmy* rats were functionally defective.

Rescue of *dmy/dmy* mutant phenotypes by transgenic complementation

To ascertain that the molecular defect (*i.e.* G-to-A transition) observed in the *dmy* mutant haplotype was causative of the abnormal phenotype observed in *dmy/dmy* rats, we attempted to rescue the mutant phenotype by transgenic complementation. We

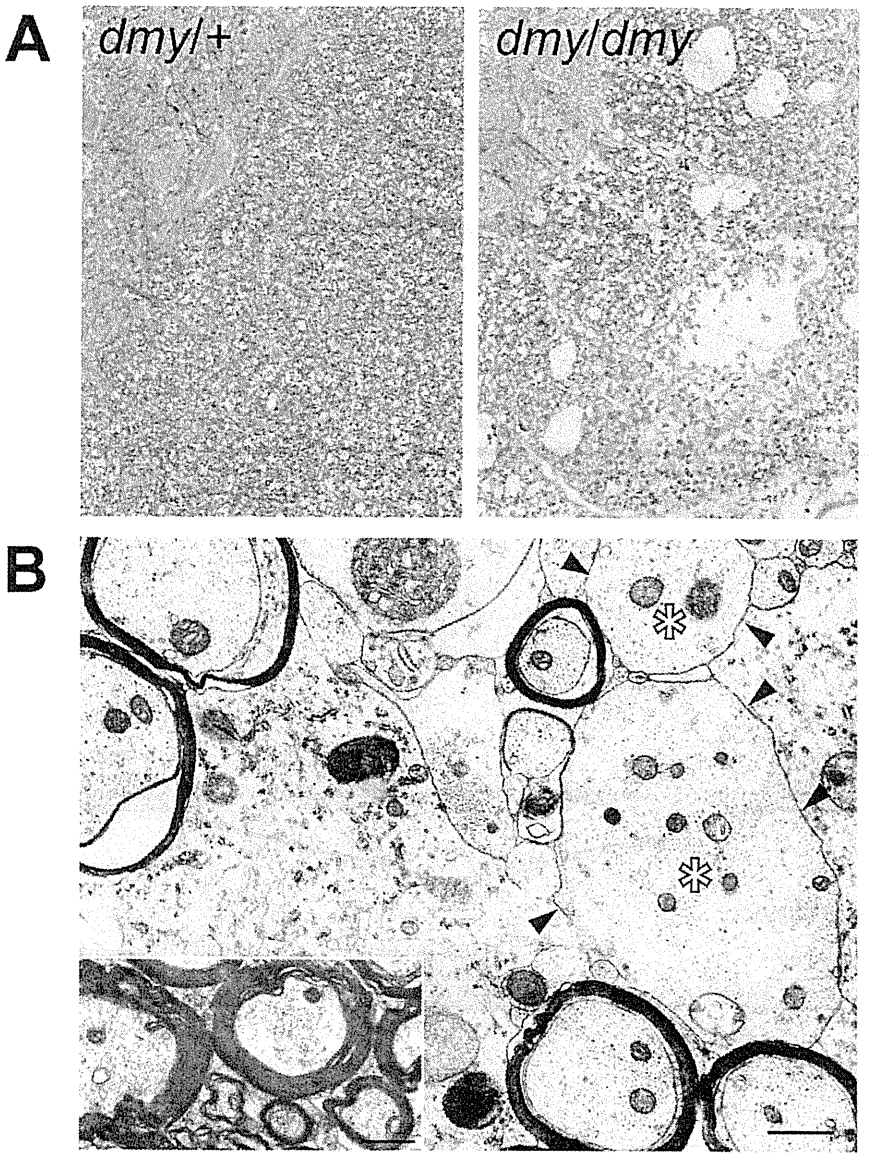

Figure 1. Demyelination in *dmy/dmy* rats. A. Histopathology of the cervical part of the spinal cord of *dmy/+* (left) and *dmy/dmy* (right) rats aged 10 weeks. Luxol fast blue-HE staining. Original magnification: ×100. B. Electron microscopy of the cervical part of spinal cord of *dmy/dmy* rats (10 weeks). Naked axons with demyelination (arrowheads) are indicated by asterisks. Inset: control image of the spinal cord from the age-matched wild type rat. Axons are normally myelinated. Bar = 1 μm.
doi:10.1371/journal.pgen.1001262.g001

established two independent WTC.DMY-*dmy* lines, expressing each *Mrs2* wild-type cDNA under the control of a cytomegalovirus (CMV) promoter (Figure S2A), and found that all *dmy/dmy* transgenic rats exhibited a completely normal phenotype, with no paralysis of the hind limbs. Histopathological analyses demonstrated that both transgenic lines no longer exhibited any sign of demyelination of the CNS (Figure S2B). In addition, lactic acid levels of the cerebrospinal fluid of transgenic *dmy/dmy* rats had returned to the normal range (Figure S2C). Electron microscopic observations revealed that mitochondria of the oligodendrocytes in transgenic rats were normal in their morphology and number (Figure S2D). These findings confirmed that the molecular changes reported above and observed in the *Mrs2* gene were indeed causative of the *dmy*-mutant phenotypes. For this reason we decided that the symbol of the mutant allele should, from now on, be changed to $Mrs2^{dmy}$.

MRS2-GFP recombinant protein is expressed in the mitochondria

To characterize the tissues and cell types expressing MRS2 as well as the subcellular localization of this protein in the CNS, we generated a strain of rats transgenic for a recombinant MRS2-GFP BAC clone. These transgenic rats were expected to express recombinant protein under the control of the endogenous, normal *Mrs2* promoter. We found that cytoplasmic dot-like MRS2-GFP

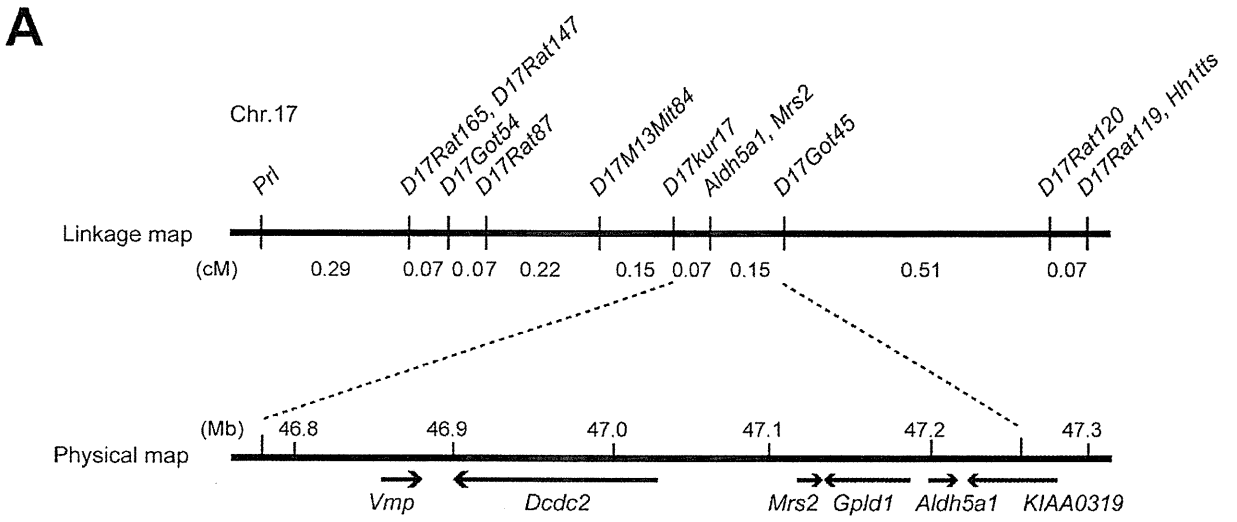
A
Chr.17
Prl
D17Rat165, D17Rat147
D17Got54
D17Rat87
D17M13Mit84
D17kur17
Aldh5a1, Mrs2
D17Got45
D17Rat120
D17Rat119, Hh1tts
Linkage map
(cM)
0.29
0.07 0.07
0.22
0.15 0.07 0.15
0.51
0.07
(Mb)
46.8
46.9
47.0
47.1
47.2
47.3
Physical map
Vmp
Dcdc2
Mrs2 Gpld1 Aldh5a1 KIAA0319

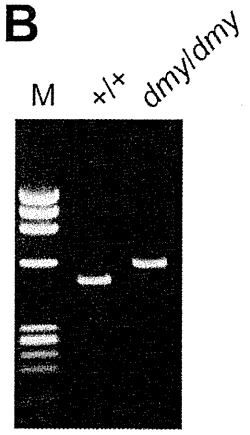
B
M
+/+
dmy/dmy

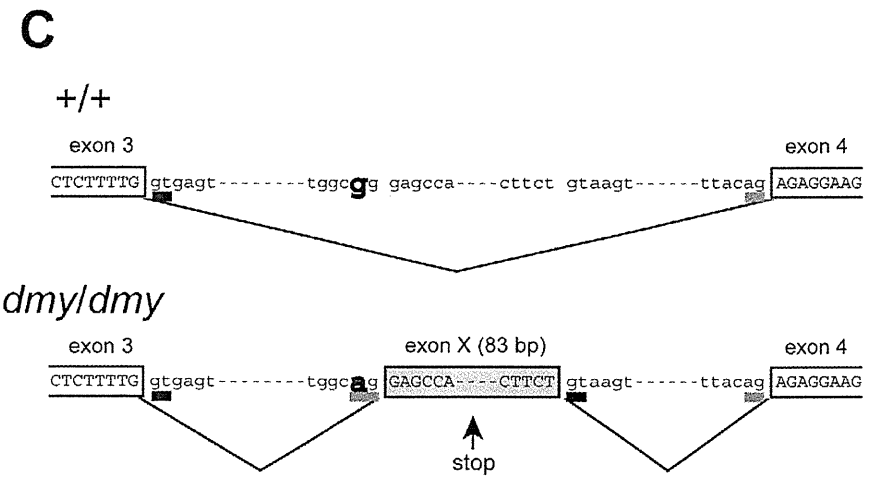
C
+/+
exon 3
exon 4
CTCTTTTG gtgagt--------tggcgg gagcca----cttct gtaagt------ttacag AGAGGAAG
dmy/dmy
exon 3
exon X (83 bp)
exon 4
CTCTTTTG gtgagt--------tggcag GAGCCA----CTTCT gtaagt------ttacag AGAGGAAG
stop

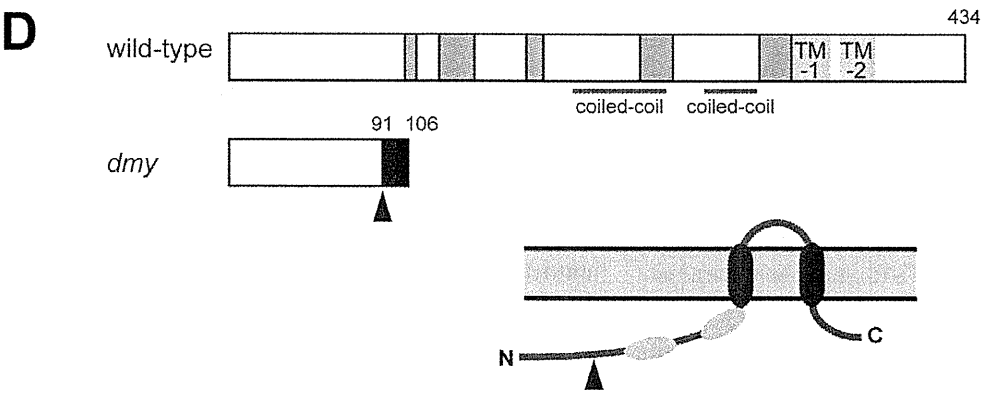
D
wild-type
434
TM -1
TM -2
coiled-coil
coiled-coil
dmy
91 106
N
C

Figure 2. Positional cloning of the *dmy* mutation. A. The *dmy* locus was localized within a 0.22-cM region of chromosome 17 between *D17Kur17* and *D17Got45* and no recombination was observed with SSLP markers designed from *Aldh5a1* and *Mrs2* genomic sequences in 1,374 informative meioses. Within the 0.48-Mb physical interval between *D17Kur17* and *D17Got45*, harboring the *dmy* locus, 6 genes: *Vmp* (vesicular membrane protein p24), *Dcdc2* (doublecortin domain containing 2), *Mrs2* (MRS2 magnesium homeostasis factor (*S. cerevisiae*), *Gpld1* (glycosylphosphatidylinositol specific phospholipase D1), *Aldh5a1* (aldehyde dehydrogenase family 5, subfamily A1), and *KIAA0319*, were previously mapped. B. A larger RT-PCR product was obtained when amplifying the 5′ region of *Mrs2* cDNAs from *dmy/dmy* rats with a primer set of rMrs2I-3&4 (5′-TGTACTGATCTACCCGAGTTCC-3′ and 5′-TCTGGAGTTATCACAGCCTTCA-3′). M: molecular marker, ΦX174-*Hae*III digest. C. Upper: Genomic organization in the vicinity of intron 3 of the *Mrs2* wild-type allele. Lower: Genomic rearrangements in the same intron 3 of the $Mrs2^{dmy}$ mutant allele. In the $Mrs2^{dmy}$ mutant allele, a novel splice acceptor site was generated as a consequence of a G-to-A transition at 177 bp downstream of the end of exon 3. An 83-bp genomic sequence (boxed in gray), downstream of the recently generated acceptor site (tggcag), is then inserted into the *Mrs2* mutant transcript. This sequence contains a premature stop codon (vertical arrow), which truncates the protein almost immediately downstream of exon 3. D. Schematic representations of the wild-type and *dmy* MRS2 proteins. Conserved amino acid residues and transmembrane domains are indicated by grey and purple boxes, respectively. Coiled-coil regions are indicated by horizontal orange lines. The position of the *dmy* mutation is indicated by an arrowhead, and the additional 15 residues (GATWTPRILEECLES), indicated by a black box, are deduced to be added subsequently. Bottom: Schematic representation of the topology of MRS2. Purple: transmembrane domains, Orange: coiled-coil regions. The position of the *dmy* mutation is indicated by an arrowhead.
doi:10.1371/journal.pgen.1001262.g002

signals were observed in neurons throughout the CNS. To a lesser extent, astrocytes and oligodendrocytes also exhibited occasional expression of MRS2 (Figure S3). Confocal microscopy demonstrated that MRS2 is located in the mitochondria (Figure 4A–4C). Moreover, immunoelectron microsopic examinations with anti-GFP antibody revealed that MRS2 is localized in the inner membrane of the mitochondria (Figure 4D). MRS2 expression was also observed in the myocardium, liver, testis and skeletal muscles (Figure S4).

Microglia activation and high expression of inflammatory cytokines were observed in $Mrs2^{dmy}/Mrs2^{dmy}$ rats

Microglial activation, characterized by cellular hypertrophy, has been reported in various dysmyelinating and demyelinating pathologies. To assess microglial activation, we performed immunohistochemistry for IBA1, a specific marker of microglia. In $Mrs2^{dmy}/Mrs2^{dmy}$ rats, prolonged activation of microglia was prominently observed at 6–7 weeks of age (Figure 5A and 5B), the stage at which clinical symptoms such as flaccid paralysis were commonly observed. Expression levels of proinflammatory cytokines, such as *Il1b* and *Il6*, were also significantly higher in $Mrs2^{dmy}/Mrs2^{dmy}$ rats than in wild-type littermates at 6 weeks of age (Figure 5C).

Discussion

Characterization, by positional cloning, of the molecular defect responsible for the demyelinating phenotype observed in adult *dmy/dmy* rats led us to incriminate a mutation in the *Mrs2* gene. No mutant allele before $Mrs2^{dmy}$, which we report here, has ever been reported at this locus in any mammalian species.

Mrs2 encodes an inner membrane Mg^{2+} channel in mitochondria and belongs to a family with orthologous copies in a wide range of species [10,12]. *Mrs2* was originally identified in yeast, and orthologous copies of this gene have been identified in a variety of organisms, including bacteria (CorA), fungi (Alr1), and plants (AtMrs2). All proteins in the family have the same substrate selectivity: they transport Mg^{2+}, Co^{2+} and some other divalent cations across the mitochondrial membrane. Even if these proteins exhibit relatively low sequence similarities, they all have a few important domains at the same relative position and can functionally complement each other over a wide range of phylogenetic distances [16,17]. In mammals, the normal protein MRS2 has two universally conserved transmembrane domains (TMs) and a conserved Gly-Met-Asn (GMN) motif close to the first TM domain that forms part of the pore and is essential for Mg^{2+} transport [18] (Figure 2D, Figure S5). As we demonstrated, the protein is truncated in *dmy/dmy* mutant rats, having lost both of its essential domains and accordingly its function of an Mg^{2+} transmembrane transporter. In other words, $Mrs2^{dmy}$ is a null allele, which is totally consistent with its recessive allelic interaction.

An MRS2 is a major transport for Mg^{2+} uptake into mitochondria, its function would be expected to be important, if not essential, for the maintenance of respiratory complex I and accordingly for cell viability [6,11]. This assumption was supported by the analysis of MRS2 knock-down, mediated by shRNA in a human HEK-293 cell line, which resulted in a series of physiological changes ranging from transient reduction of Mg^{2+} uptake to the complete loss of mitochondrial respiratory complex I, with decreased mitochondrial membrane potential and cell death, depending on the duration of knock-down treatment [11]. However, if we consider the phenotype of our mutant rat, which is apparently limited to the myelination process with a rather long lifespan, the role of MRS2 in the maintenance of cell integrity should be reconsidered.

Considering the pathological features that appear to be characteristics of the $Mrs2^{dmy}$ allele on the one hand, and MRS2-specific functions, as described above on the other, it is logical to consider that the demyelinating syndrome in mutant rats results from a mitochondrial disease. This assertion is supported by the observation of an elevated rate of lactic acid in the cerebrospinal fluid, reduced ATP in the brain, increased COX activity, and the morphological alteration of mitochondria, which is generally considered a major characteristic of mitochondrial diseases [13–15]. An increase in mitochondria is characteristic of cells with reduced respiratory capacity [19]. The association of mitochondrial dysfunction with demyelination (or leukodystrophy) has been already reported in Leigh syndrome and mitochondrial DNA depletion syndrome [20–23]. The tissues most frequently affected in these mitochondrial diseases are the cerebrum, peripheral nerves, and skeletal muscles, presumably because cells of these tissues require more energy than any other cells in the body. Unfortunately, the detailed pathophysiological mechanism(s) leading to demyelination in these diseases has not yet been unraveled. We consider that our mutant rat could be an interesting tool for investigating this matter.

Mitochondrial dysfunction has also been observed in multiple sclerosis (MS), one of the most common demyelination diseases, but here again many aspects of the pathophysiology require further investigation [24,25]. This difficulty of linking gene functions with a specific syndrome is not so surprising if we consider that, according to the most recent estimates, there may be as many as 1,500 nuclear-encoded mitochondrial proteins [26] and that less than half have been identified with experimental support. Clearly, a complete protein inventory of this organelle

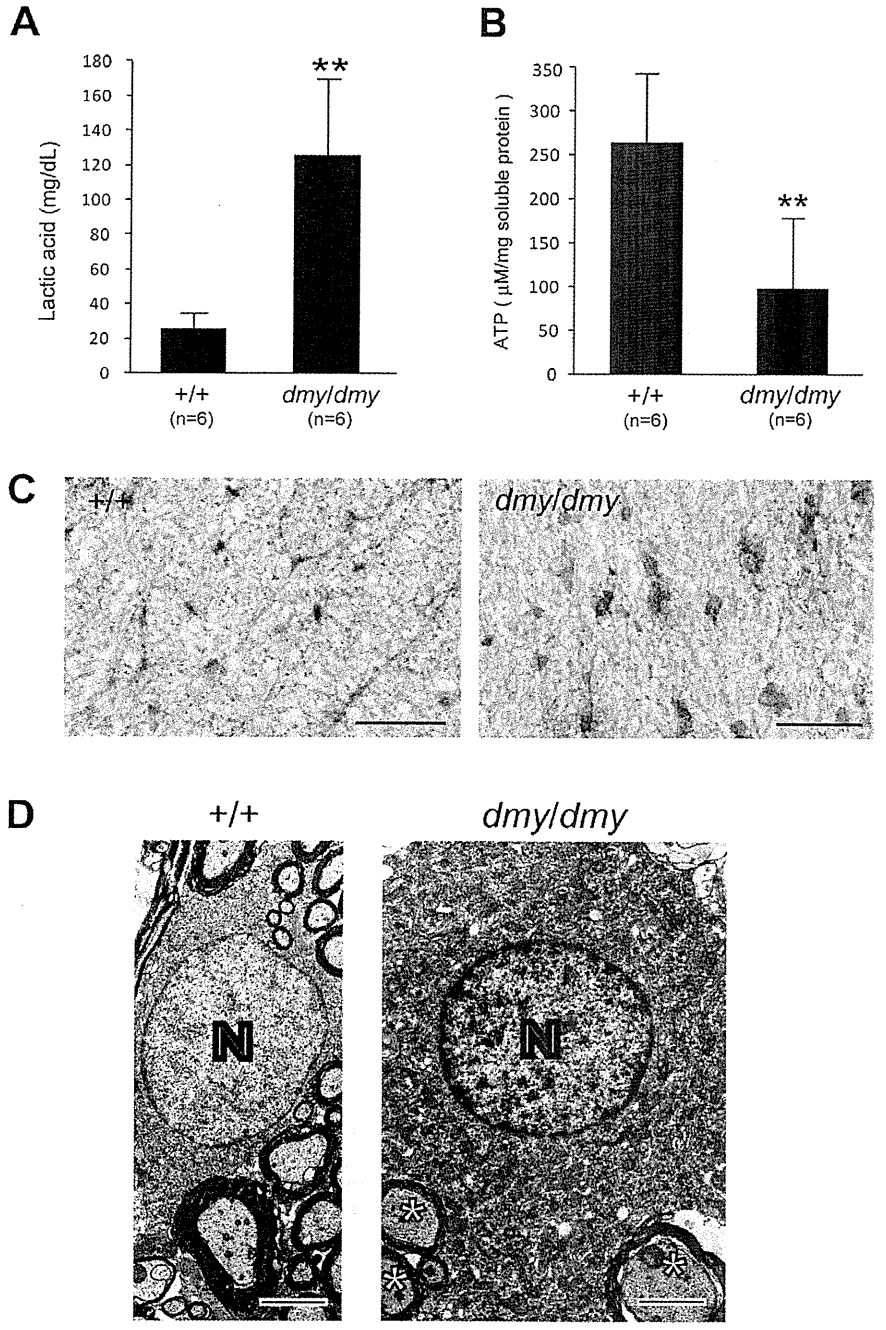

Figure 3. Biochemical and morphological abnormalities in the mitochondria of *dmy/dmy* mutant rats. A. Lactic acid concentration in cerebrospinal fluid of 6–7-week-old *dmy/dmy* rats and age-matched wild-type rats. **, P<0.002. B. ATP levels in the brain of 6–7-week-old *dmy/dmy* rats and age-matched wild-type rats. **, P<0.005. C. Cytochrome oxidase staining of the spinal cords of 6–7-week-old *dmy/dmy* (right) and age-matched wild-type (left) rats. Swollen oligodendrocytes were often seen they showed increased COX reaction product. Bar = 50 μm. D. Electron microphotographs of a swollen oligodendrocyte in a *dmy/dmy* rat (right) and an oligodendrocyte in a control wild-type rat. White matter of thoracic spine at 6 weeks of age. N: Nucleus of the oligodendrocyte. Axons adjacent to the oligodendrocyte are indicated by asterisks. Bar = 2 μm.
doi:10.1371/journal.pgen.1001262.g003

across tissues would provide a molecular framework to relate mitochondrial biology and pathogenesis [27].

A point concerning *Mrs2* gene expression in the CNS that is worth noting after our experiments and observations is that the gene in question is expressed at a higher rate in neurons than in oligodendrocytes (Figure 4, Figure S3). This was rather unexpected if we consider that oligodendrocytes are the cells actually responsible for myelination of the CNS. At this time, it remains

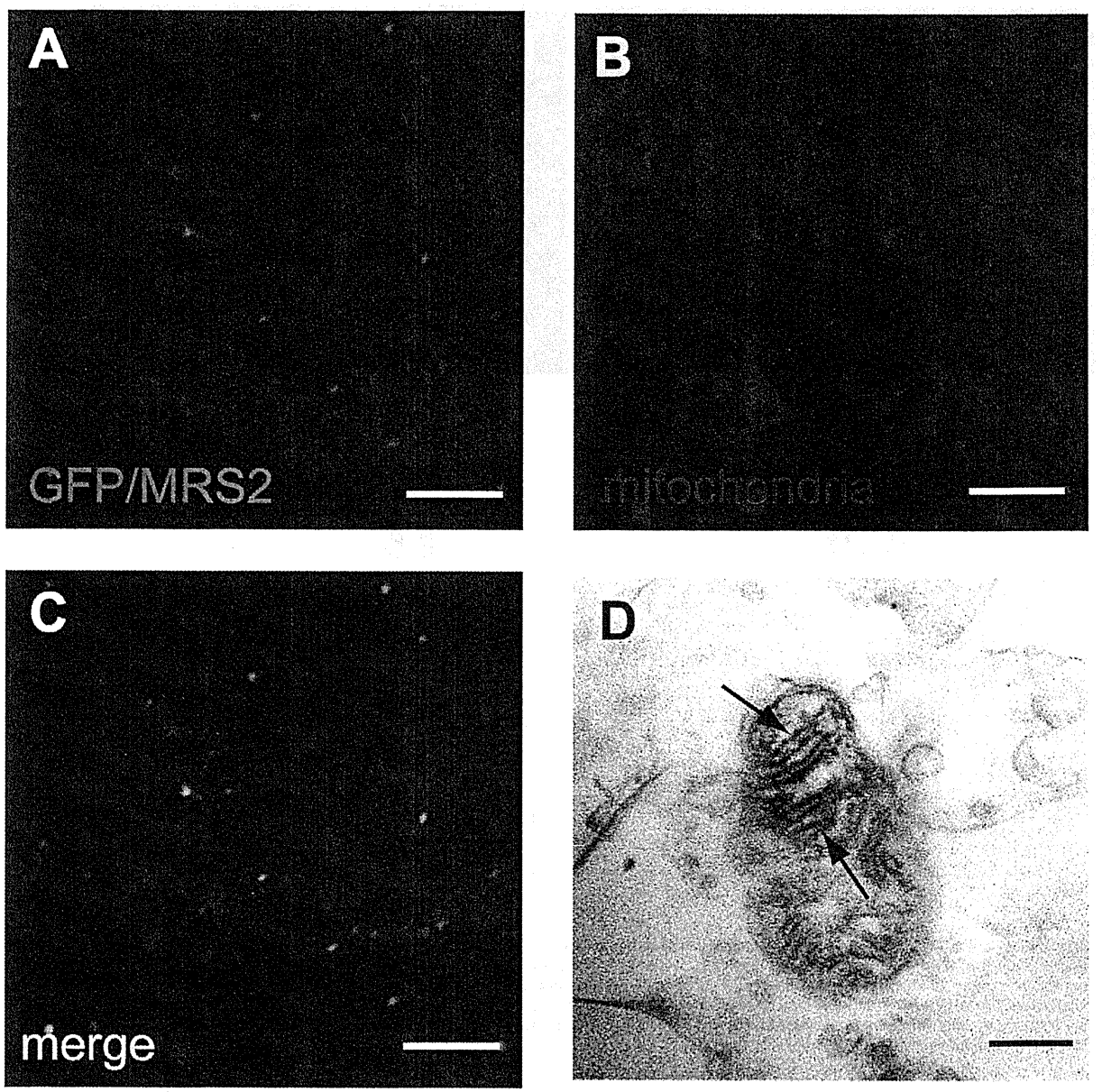

Figure 4. Expression of MRS2 protein in the mitochondria. MRS2-GFP recombinant protein (Green) was seen in the cytoplasm of pyramidal cells (A). MRS2-GFP signals were colocalized with the mitochondria (B), as shown in the confocal image of GFP and mitochondrial immunohistochemistry (C). Nuclei were stained with DAPI (Blue). Bar: 5 μm. Immunoelectron microscopy using anti-GFP antibody revealed that MRS2-GFP signals were localized in the inner membrane of the mitochondria (arrows) (D). Bar: 200 nm.
doi:10.1371/journal.pgen.1001262.g004

unclear whether the demyelination in *dmy/dmy* rats is triggered cell-autonomously or cell-nonautonomously. Instead, it is likely that demyelination is enhanced by the surrounding cells, such as activated microglia and astroglia. At 6 weeks of age, when *dmy/dmy* rats began to exhibit ataxia [9], cytokine levels were elevated and microglia were activated (Figure 5), and it is considered that activated microglia cause neuronal damage through the release of potentially cytotoxic molecules, such as proinflammatory cytokines, reactive oxygen intermediates, proteinases, and complement proteins [28]. Oligodendrocytes show greater vulnerability to such molecules [29,30]. Additionally, Kuwamura and co-workers reported prominent astrogliosis and many ED-1-positive macrophages in myelin-destroyed areas [9]. When considered together, these morphological observations led us to believe that the demyelination observed in *dmy/dmy* rats is probably enhanced by activated microglia and astroglia.

In summary, we identified $Mrs2^{dmy}$ as a loss-of-function mutation of the *Mrs2* gene that normally encodes Mg^{2+} transporter protein of the mitochondrial inner membrane. Our observations also demonstrate that the mechanisms underlying the

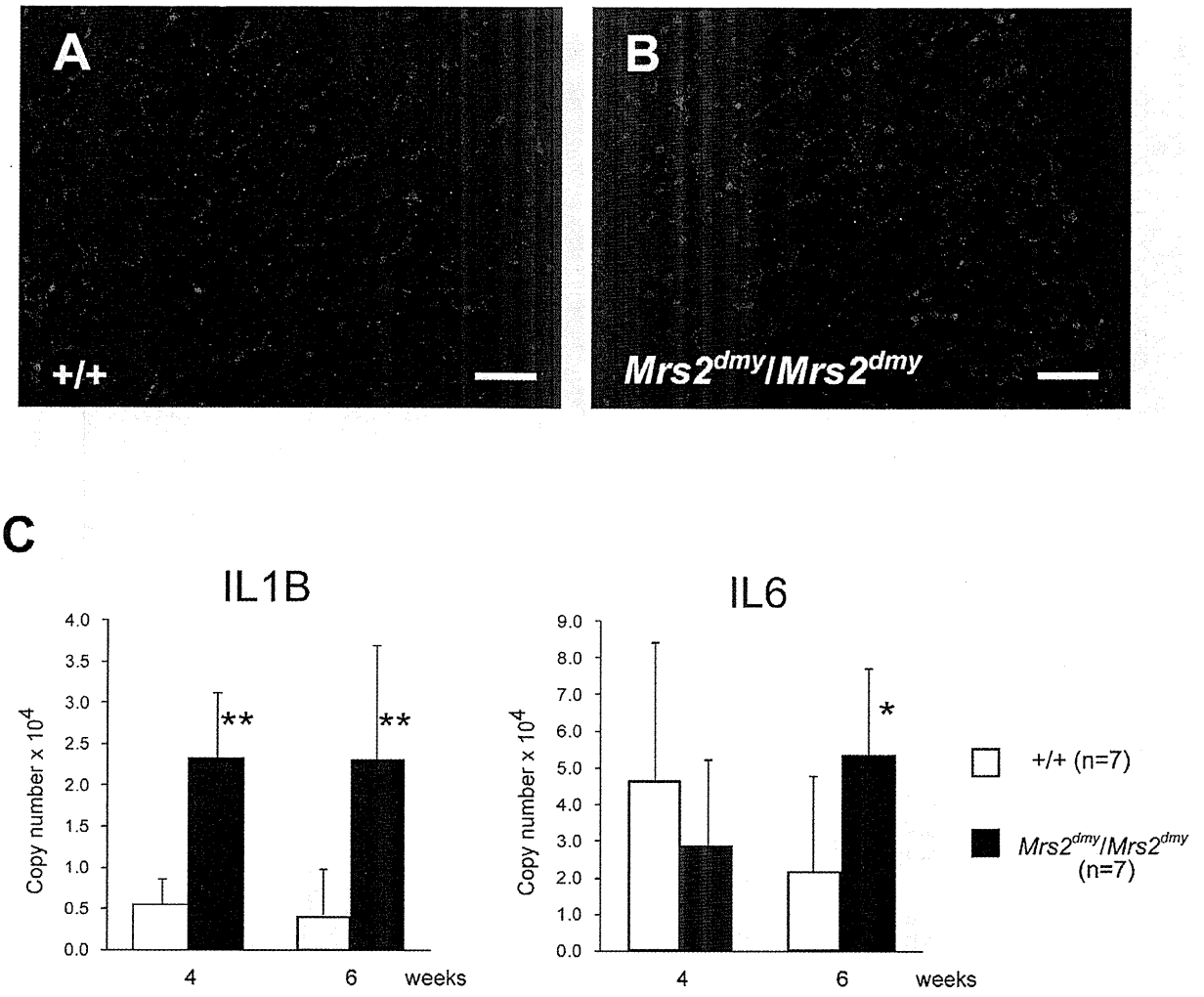

Figure 5. Activation of microglia in the central nervous system of *Mrs2*^{dmy}/*Mrs2*^{dmy} rats. Immunohistochemistry for Iba1 in the lumbar part of the spinal cord of wild-type (A) and *Mrs2*^{dmy}/*Mrs2*^{dmy} rats (B) at 6 weeks of age. Signals of Iba1 (AlexaFluor 546 nm; red), which is upregulated during the activation of microglia, are seen in *Mrs2*^{dmy}/*Mrs2*^{dmy} rats much more the wild-type control. Nucleus is stained with DAPI (blue). C, Inflammatory cytokine mRNA expression in the CNS of wild-type (□) and *Mrs2*^{dmy}/*Mrs2*^{dmy} (■) rats. IL1b expression was elevated in *Mrs2*^{dmy}/*Mrs2*^{dmy} rats at 4 and 6 weeks of age. IL6 was elevated in *Mrs2*^{dmy}/*Mrs2*^{dmy} rats at 6 weeks of age. * $P<0.05$, ** $P<0.005$.
doi:10.1371/journal.pgen.1001262.g005

initial development of myelin (myelination) are different from those that are involved in its maintenance and turnover since, in *Mrs2*^{dmy}/*Mrs2*^{dmy} rats, myelin development is normal while its maintenance is defective. Our mutant rats also appear to be an excellent animal model, not only to evaluate the causal relationships between primary mitochondrial dysfunction and subsequent demyelination, but also for the development of therapies making use, for example, of cell transplantation.

Materials and Methods

Genetic fine mapping of *dmy*

Congenic strains WTC (NBRP#0020) and WTC.DMY-*dmy* (NBRP#0021) were both from the National BioResource Project - Rat, Kyoto University (Kyoto, Japan). (WTC.DMY-*dmy* × BN/SsNSlc)F1(+/*dmy*) rats were intercrossed to produce F2 progeny. *dmy*/*dmy* homozygotes were identified at 7–8 weeks of age, when paralysis of the hind limbs was obvious. 687 *dmy*/*dmy* rats were collected out of 3,252 F2 animals (~21%) and used for fine mapping of the *dmy* locus. Simple sequence length polymorphisms (SSLPs) from the *Prl* (prolactin) and *Hh1tts* (Testis-specific histone, H1t and H4t) genes were used for genotyping as described [31]. To refine the limits of the recombinant interval between *Prl* and *Hh1tts*, two gene-specific and one anonymous SSLP markers were used: *Mrs2* (5′-TCTCCCTTGCCTCTATCTCTCGTCT-3′,5′-CCTGCAGTACTGGGTAAGCCTGATG-3′), *Aldh5a1* (5′-GTTAACTGCACAAGAGCAAGCCAGT-3′, 5′-GCTAATGTTAAGTCATGGGGTGAGG-3′), and *D17Kur17* 5′-ACCTCTTTTTGCCAGCATTG-3′, 5′-CCCTGGGATTGGTCCATA-3′).

All animal experiments were approved by the Animal Research Committee of Kyoto University and were conducted according to the Regulations on Animal Experimentation of Kyoto University.

RT-PCR and direct sequencing

Total RNA was isolated from the brain of 5-week-old animals using ISOGEN (NIPPON GENE, Tokyo, Japan). RT-PCR and direct sequencing of the PCR products were carried out as described previously [32].

Transgenic rescue and recombinant BAC transgenics

A construct containing the CMV promoter, 1.45-kb of the *Mrs2* coding sequence, and SV40 polyA signal was excised from the vector (pCMV-Script; Agilent Technologies, CA, USA) and used as a transgene, which was microinjected into the pronuclei of fertilized oocytes collected from Crj:Wistar rats. Transgenic offspring founder rats were then crossed with WTC- +/*dmy* rats and then backcrossed again to WTC- +/*dmy* rats to obtain *dmy*/*dmy* homozygous and also hemizygous for the transgene (*dmy*/*dmy*, tg/-). Expression of the transgene was confirmed by RT-PCR with primers (5′-GCGAATGGAGATCCAATTTT-3′, 5′-GGGAG-GTGTGGGAGGTTTT-3′) to detect SV40 polyA sequence. Brain RNA was treated with DNase I (New England BioLabs) to remove contaminating genomic DNA and then subjected to cDNA synthesis.

A rat BAC clone, CHORI-230-9K13, including the rat *Mrs2* gene was modified to express MR2SL-EGFP fusion protein under the endogenous promoter by ET recombination technology [33]. Modified genomic DNA was excised from the vector and then used for *in ovo* transgenesis.

Quantitative PCR

Real-time PCR was performed using the Thermal Cycler Dice Real Time System (Takara Bio Inc., Otsu, Japan) with SYBR Premix Ex Taq II (Takara Bio Inc., Otsu, Japan). By monitoring amplification curves of a test sample and reference samples that contained 101–106 molecules of the gene of interest, the number of target molecules in the test sample was analyzed. The number of target molecules was normalized to that of glyceraldehyde-3-phosphate dehydrogenase (*Gapdh*) as an internal control. The primers used are as follows: 5′-GCTGTGGCAGCTACC-TATGTCTTG-3′ and 5′-AGGTCGTCATCATCCCACGAG-3′ for the rat Interleukin-1b (*Il1b*), 5′-CCACTTCACAAGTCG-GAGGCTTA-3′ and 5′-GTGCATCATCGCTGTTCATACA-ATC-3′ for the rat interleukin-6 (*Il6*), 5′-GGCACAGT-CAAGGCTGAGAATG-3′ and 5′-ATGGTGGTGAAGACGC-CAGTA-3′ for rat *Gapdh*.

Electron microscopy

Perfusion fixation through the left ventricle was conducted with 4% paraformaldehyde in 0.1 M phosphate buffer (PB). Brains and spinal cords were dissected and stored in 2% paraformaldehyde and 2.5% glutaraldehyde in 0.1 M PB, then post-fixed with 2% osmic acid for 2 hours and embedded in epoxy resin. Ultrathin sections were double-stained with uranyl acetate and lead citrate and examined by a Hitachi H-7500 electron microscope (Hitachi, Tokyo, Japan).

Immunohistochemistry

Immunohistochemistry was performed as described previously [9]. The following primary antibodies were used: monoclonal anti-2′, 3′-cyclic nucleotide-3′-phosphodiesterase (CNPase) for oligodendrocytes (1:1,000; Sigma, St. Louis, MO, USA), monoclonal anti-mitochondria (1:100; Abcam, Cambridge, MA, USA), polyclonal anti-GFAP for astrocytes (1:1,000; Dako, Carpinteria, CA, USA), polyclonal anti-Iba1 for microglia/macrophages (1:200; Wako Pure Chemical Industries, Osaka, Japan). Cy3-conjugated anti-mouse IgG (1:500; Jackson Laboratories) or Alexa 588-conjugated anti-rabbit IgG (1:500; Molecular Probes) antibody was reacted. Nuclei were counterstained with DAPI (Vactor Laboratories). Signals were detected with a fluorescence microscopy (Olympus, Tokyo, Japan) or a confocal imaging system (C1Si; Nikon, Tokyo, Japan).

For immunoelectron microscopy, PFA-perfused frozen sections were incubated with rabbit antibody against fluorescent protein (1:2,000; Molecular Probes) at 4 °C overnight. After washing in PBS, peroxidase-conjugated anti-rabbit IgG Fab fraction (Jackson Laboratories, 1:1,000) and immunoreactions were reacted 3,3-diaminobenzidine substrate kit (Vector Laboratories), postfixed in 1% osmium tetraoxide, dehydrated in graded ethanol, and then embedded in epoxy resin. Ultrathin sections were examined by electron microscopy (Hitachi, Tokyo, Japan).

Lactic acid measurements

Cerebrospinal fluid was collected from *dmy*/*dmy*, wild-type littermates, and *dmy*/*dmy* with the normal *Mrs2* transgene at 6–7 weeks of age under isoflurane anesthesia. They were then mixed with 0.8N perchloric acid to inactivate proteins. After centrifugation, lactic acid concentrations of the supernatants were measured by Determiner LA (KYOWA MEDEX Co., Ltd., Tokyo, Japan).

Cytochrome oxidase histochemistry

Frozen spinal cord sections were prepared. Then, 100 µl of freshly prepared reaction buffer [50 mM Tris/HCl (pH 7.4), 0.5 mg/ml diaminobenzidine, 20 µg/ml catalase and 0.50 mg/ml cytochrome C] was added to each section and slides were incubated for 30 min at 37°C.

ATP measurements

Rats were sacrificed by cervical dislocation and the brains were immediately excised, frozen in liquid nitrogen, and stored at −80°C until measurement. In order to release cellular ATP, frozen tissue (25 mg) was boiled for 2 min after the addition of 300 µl water containing 100 mM Tris/HCl (pH 7.75) and 4 mM EDTA. Samples were placed on ice and homogenized by sonification (micro tip, 1 s ×10 pulse). ATP concentrations were determined using the ATP bioluminescence assay kit HS II (Roche) according to the manufacturer's protocol. Data were standardized to the protein concentration which was determined by Coomassie Plus – the better Bradford assay kit (Pierce).

Statistical analysis

Statistical differences in lactic acid, ATP and mRNA expressions between wild-type and *dmy*/*dmy* rats were evaluated using the Mann-Whitney U test.

Supporting Information

Figure S1 Detection of the $Mrs2^{dmy}$ mutation. A. Chromatograms showing the $Mrs2^{dmy}$ G-to-A mutation. Upper: wild-type genome. Lower: $Mrs2^{dmy}/Mrs2^{dmy}$ genome. The $Mrs2^{dmy}$ mutation disrupted *Aci*I restriction site (GGCG) in the $Mrs2^{dmy}/Mrs2^{dmy}$ genome. B. Molecular diagnosis of the $Mrs2^{dmy}$ mutation. In the wild type, the 349-bp PCR product amplified with primers rMrs2-31&32 (5′-AAAGTTTGACAAAGAAGGAAACG-3′ and 5′-GGGGATGGAGGGCTATGTAA-3′) is digested with *Aci*I but not in $Mrs2^{dmy}/Mrs2^{dmy}$ mutant rats. M: ΦX174-*Hae*III digests.
Found at: doi:10.1371/journal.pgen.1001262.s001 (1.15 MB TIF)

Figure S2 Transgenic rescue experiment. A. Expression of the transgene in the brain of a transgenic rat. Brain cDNA from Tg-

positive rats (Lanes 2 and 3) and Tg-negetive rats (Lanes 1and 4) was used as templates. Brain RNA was treated with DNaseI to remove contaminating genomic DNA. M: ΦX174 *Hae*III digests. B. Histopathology of the cervical part of the spinal cord of *dmy/dmy* transgene-negative rats (left) and *dmy/dmy* transgene-positive (right) rats aged 10 weeks. Luxol fast blue-HE staining. Original magnification: ×100. C. Lactic acid concentration in cerebrospinal fluid of 6-7-week-old *dmy/dmy* rats and age-matched *dmy/dmy Mrs2* cDNA-transgenic rats. Elevated lactic acid (126 ± 43.7 mg/dL) was reduced to normal level (22 ± 3.1 mg/dL). **, $P < 0.002$. D. Electron microphotograph of an oligodendrocyte in a *dmy/dmy* transgene-positive rat. Densely packed mitochondria (arrowheads) were found in the cytoplasm. Bar: 2μm.
Found at: doi:10.1371/journal.pgen.1001262.s002 (5.52 MB TIF)

Figure S3 MRS2 expression in the CNS of Mrs2-GFP recombinant BAC transgenic rats. MRS2 signals were mainly found in neurons (A), and occasionally in GFAP-positive astrocytes (B) and CNP-positive oligodendrocytes (C). Left: Bar: 50 μm. Center, Right: Bar: 20 μm.
Found at: doi:10.1371/journal.pgen.1001262.s003 (3.15 MB TIF)

Figure S4 MRS2 expression in Mrs2-GFP recombinant BAC transgenic rats. MRS2 signals were observed in the myocardium (A), liver (B), testis (C) and skeletal muscles (D). Bar: 50 μm.
Found at: doi:10.1371/journal.pgen.1001262.s004 (6.29 MB TIF)

Figure S5 Sequence alignment of yeast, human, and rat MRS2 proteins. Predicted transmembrane domains (TM-1, TM-2) are boxed; * indicates identical residues; : indicates conservative substitution; . indicates semiconservative substitutions. The sequence of a motif conserved in all putative magnesium transporters, G-M-N, is indicated in bold. Predicted coiled-coil regions are underlined, five regions with conserved amino acid residues (CRB-1-5; conserved residue block) are shaded grey. Arrowhead: The position of the residue affected by the *dmy* mutation, after which the 15 additional residues follow in mutant MRS2.
Found at: doi:10.1371/journal.pgen.1001262.s005 (1.38 MB TIF)

Acknowledgments

The authors are grateful to M. Yokoe for excellent technical assistance.

Author Contributions

Conceived and designed the experiments: TK. Performed the experiments: TK MK ST TI YN KK. Analyzed the data: TK MK. Contributed reagents/materials/analysis tools: MA TS. Wrote the paper: TK MK JLG.

References

1. Werner H, Jung M, Klugmann M, Sereda M, Griffiths IR, et al. (1998) Mouse models of myelin diseases. Brain Pathol 8: 771–793.
2. Griffiths IR (1996) Myelin mutants: model systems for the study of normal and abnormal myelination. Bioessays 18: 789–797.
3. Meyer Zu Horste G, Nave KA (2006) Animal models of inherited neuropathies. Curr Opin Neurol 19: 464–473.
4. Kuramoto T, Sotelo C, Yokoi N, Serikawa T, Gonalons Sintes E, et al. (1996) A rat mutation producing demyelination (*dmy*) maps to chromosome 17. Mamm Genome 7: 890–894.
5. Kitada K, Guenet JL, Serikawa T (2000) Determination of the mouse homologous region for the rat *dmy* locus. J Exp Anim Sci 41: 40–43.
6. Schindl R, Weghuber J, Romanin C, Schweyen RJ (2007) Mrs2p forms a high conductance Mg^{2+} selective channel in mitochondria. Biophys J 93: 3872–3883.
7. Gregan J, Bui DM, Pillich R, Fink M, Zsurka G, et al. (2001) The mitochondrial inner membrane protein Lpe10p, a homologue of Mrs2p, is essential for magnesium homeostasis and group II intron splicing in yeast. Mol Gen Genet 264: 773–781.
8. Schock I, Gregan J, Steinhauser S, Schweyen R, Brennicke A, et al. (2000) A member of a novel Arabidopsis thaliana gene family of candidate Mg^{2+} ion transporters complements a yeast mitochondrial group II intron-splicing mutant. Plant J 24: 489–501.
9. Kuwamura M, Kanehara T, Tokuda S, Kumagai D, Yamate J, et al. (2004) Immunohistochemical and morphometrical studies on myelin breakdown in the demyelination (*dmy*) mutant rat. Brain Res 1022: 110–116.
10. Kolisek M, Zsurka G, Samaj J, Weghuber J, Schweyen RJ, et al. (2003) Mrs2p is an essential component of the major electrophoretic Mg^{2+} influx system in mitochondria. Embo J 22: 1235–1244.
11. Piskacek M, Zotova L, Zsurka G, Schweyen RJ (2009) Conditional knockdown of hMRS2 results in loss of mitochondrial Mg^{2+} uptake and cell death. J Cell Mol Med 13: 693–700.
12. Wiesenberger G, Waldherr M, Schweyen RJ (1992) The nuclear gene MRS2 is essential for the excision of group II introns from yeast mitochondrial transcripts in vivo. J Biol Chem 267: 6963–6969.
13. Devivo DC (1993) The expanding clinical spectrum of mitochondrial diseases. Brain Dev 15: 1–22.
14. Huttemann M, Zhang Z, Mullins C, Bessert D, Lee I, et al. (2009) Different proteolipid protein mutants exhibit unique metabolic defects. ASN Neuro 1.
15. Thambisetty M, Newman NJ (2004) Diagnosis and management of MELAS. Expert Rev Mol Diagn 4: 631–644.
16. Bui DM, Gregan J, Jarosch E, Ragnini A, Schweyen RJ (1999) The bacterial magnesium transporter CorA can functionally substitute for its putative homologue Mrs2p in the yeast inner mitochondrial membrane. J Biol Chem 274: 20438–20443.
17. Zsurka G, Gregan J, Schweyen RJ (2001) The human mitochondrial Mrs2 protein functionally substitutes for its yeast homologue, a candidate magnesium transporter. Genomics 72: 158–168.
18. Eshaghi S, Niegowski D, Kohl A, Martinez Molina D, Lesley SA, et al. (2006) Crystal structure of a divalent metal ion transporter CorA at 2.9 angstrom resolution. Science 313: 354–357.
19. Detmer SA, Chan DC (2007) Functions and dysfunctions of mitochondrial dynamics. Nat Rev Mol Cell Biol 8: 870–879.
20. Hung PC, Wang HS (2007) A previously undescribed leukodystrophy in Leigh syndrome associated with T9176C mutation of the mitochondrial ATPase 6 gene. Dev Med Child Neurol 49: 65–67.
21. Navarro-Sastre A, Martin-Hernandez E, Campos Y, Quintana E, Medina E, et al. (2008) Lethal hepatopathy and leukodystrophy caused by a novel mutation in MPV17 gene: description of an alternative MPV17 spliced form. Mol Genet Metab 94: 234–239.
22. Spinazzola A, Viscomi C, Fernandez-Vizarra E, Carrara F, D'Adamo P, et al. (2006) MPV17 encodes an inner mitochondrial membrane protein and is mutated in infantile hepatic mitochondrial DNA depletion. Nat Genet 38: 570–575.
23. Zafeiriou DI, Koletzko B, Mueller-Felber W, Paetzke I, Kueffer G, et al. (1995) Deficiency in complex IV (cytochrome c oxidase) of the respiratory chain, presenting as a leukodystrophy in two siblings with Leigh syndrome. Brain Dev 17: 117–121.
24. Andrews HE, Nichols PP, Bates D, Turnbull DM (2005) Mitochondrial dysfunction plays a key role in progressive axonal loss in Multiple Sclerosis. Med Hypotheses 64: 669–677.
25. Mahad DJ, Ziabreva I, Campbell G, Lax N, White K, et al. (2009) Mitochondrial changes within axons in multiple sclerosis. Brain 132: 1161–1174.
26. Lopez MF, Kristal BS, Chernokalskaya E, Lazarev A, Shestopalov AI, et al. (2000) High-throughput profiling of the mitochondrial proteome using affinity fractionation and automation. Electrophoresis 21: 3427–3440.
27. Pagliarini DJ, Calvo SE, Chang B, Sheth SA, Vafai SB, et al. (2008) A mitochondrial protein compendium elucidates complex I disease biology. Cell 134: 112–123.
28. Dheen ST, Kaur C, Ling EA (2007) Microglial activation and its implications in the brain diseases. Curr Med Chem 14: 1189–1197.
29. Merrill JE, Scolding NJ (1999) Mechanisms of damage to myelin and oligodendrocytes and their relevance to disease. Neuropathol Appl Neurobiol 25: 435–458.
30. Mitrovic B, Ignarro LJ, Montestruque S, Smoll A, Merrill JE (1994) Nitric oxide as a potential pathological mechanism in demyelination: Its differential effects on primary glial cells in vitro. Neuroscience 61: 575–585.
31. Serikawa T, Kuramoto T, Hilbert P, Mori M, Yamada J, et al. (1992) Rat gene mapping using PCR-analyzed microsatellites. Genetics 131: 701–721.
32. Kuramoto T, Kitada K, Inui T, Sasaki Y, Ito K, et al. (2001) Attractin/mahogany/zitter plays a critical role in myelination of the central nervous system. Proc Natl Acad Sci U S A 98: 559–564.
33. Zhang Y, Buchholz F, Muyrers JP, Stewart AF (1998) A new logic for DNA engineering using recombination in *Escherichia coli*. Nat Genet 20: 123–128.

Kuramoto et al. BMC Genetics 2011, 12:91
http://www.biomedcentral.com/1471-2156/12/91

BMC Genetics

RESEARCH ARTICLE Open Access

A rat model of hypohidrotic ectodermal dysplasia carries a missense mutation in the *Edaradd* gene

Takashi Kuramoto*, Mayuko Yokoe, Ryoko Hashimoto, Hiroshi Hiai and Tadao Serikawa

Abstract

Background: Hypohidrotic ectodermal dysplasia (HED) is a congenital disorder characterized by sparse hair, oligodontia, and inability to sweat. It is caused by mutations in any of three Eda pathway genes: ectodysplasin (*Eda*), Eda receptor (*Edar*), and Edar-associated death domain (*Edaradd*), which encode ligand, receptor, and intracellular adaptor molecule, respectively. The Eda signaling pathway activates NF-κB, which is central to ectodermal differentiation. Although the causative genes and the molecular pathway affecting HED have been identified, no curative treatment for HED has been established. Previously, we found a rat spontaneous mutation that caused defects in hair follicles and named it sparse-and-wavy (*swh*). Here, we have established the *swh* rat as the first rat model of HED and successfully identified the *swh* mutation.

Results: The *swh/swh* rat showed sparse hair, abnormal morphology of teeth, and absence of sweat glands. The ectoderm-derived glands, meibomian, preputial, and tongue glands, were absent. We mapped the *swh* mutation to the most telomeric part of rat Chr 7 and found a Pro153Ser missense mutation in the *Edaradd* gene. This mutation was located in the death domain of EDARADD, which is crucial for signal transduction and resulted in failure to activate NF-κB.

Conclusions: These findings suggest that *swh* is a loss-of-function mutation in the rat *Edaradd* and indicate that the *swh/swh* rat would be an excellent animal model of HED that could be used to investigate the pathological basis of the disease and the development of new therapies.

Background

Hypohidrotic ectodermal dysplasia (HED) is a genetic disorder characterized by sparse hair, oligodontia, reduced sweating, and defects in a number of other ectodermal organs [1]. A lack of sweat glands can lead to recurrent severe overheating. Thus, children with HED are at substantial risk of sudden death in infancy due to fatal hyperpyrexia [2].

HED is caused by mutations in any of the three Eda pathway genes: ectodysplasin (*Eda*) [3,4], ED receptor (*Edar*) [5], and EDAR-associated death domain (*Edaradd*) [6]. They encode the ligand, receptor, and intracellular signal mediator of a single linear pathway, respectively. The Eda signaling pathway activates transcription factor NF-κB thereby playing an important role in embryonic development, especially in the development of ectodermally derived organs [1].

In humans, there are three types of HED with different inheritance: X-linked HED, autosomal dominant HED, and autosomal recessive HED. X-linked HED is the most common form of HED and is caused by mutations in *EDA*. Autosomal HED is caused by mutations in *EDAR* or *EDARADD*. Currently, over 100 different mutations in the *EDA* gene are known, while only ~20 and 4 causative mutations have been found in *EDAR* and *EDARADD*, respectively [7].

To date, four mouse models of HED are available: *Tabby, downless, Sleek*, and *crinkled*. The mutant phenotype of the *Tabby* mouse is inherited in an X-linked manner and the *Tabby* mouse carries a mutation in the *Eda* gene [4]. The recessive *downless* and dominant *Sleek* mice carry mutations in the *Edar* gene [8]. The *crinkled* mouse carries a mutation in the *Edaradd* gene [6]. The phenotypes in *Eda, Edar*, and *Edaradd* mutant mice are almost identical and include abnormalities in teeth, hair, and sweat glands, the triad of symptoms of HED. Over 20 different glands, including lacrimal, meibomian, salivary,

* Correspondence: tkuramot@anim.med.kyoto-u.ac.jp
Institute of Laboratory Animals, Graduate School of Medicine, Kyoto University, Yoshidakonoe-cho, Sakyo-ku, Kyoto 606-8501, Japan

submandibular, and mammary glands, are also affected [9-11]. These mutant mice have been used to study the roles of the Eda pathway in the development and morphogenesis of ectoderm-derived organs and to develop a novel treatment for HED using a recombinant EDA protein [12].

Mutations in some of the genes in the Eda pathway have been identified in various species, such as medaka [13], zebrafish [14], cattle [15-18], and dog [19]. Analyses of these mutations showed critical roles of the Eda pathway in the development of epithelial appendages, as well as in morphological evolution. Thus, the identification of novel mutations in different species emphasized the importance of the Eda pathway, and enabled the phenotypes of the mutated animals to be compared, giving new insights into the functions of the Eda pathway. If such novel mutations can be identified in mammals, then the affected species could be used as a disease model of HED.

In a previous study, we described a mutant rat, sparse and wavy hair (*swh*), which arose spontaneously in a colony of inbred WTC rats in 1998 [20]. The mutant phenotype is characterized by sparse and wavy hair, impaired body weight gain, and hypoplasticity of the mammary gland. The hair follicles in these rats were reduced both in number and size, a characteristic associated with hypoplasia of both the sebaceous glands and the subcutaneous fat tissues. The mammary glands of *swh/swh* female rats were hypoplastic and differentiation of mammary epithelial and myoepithelial cells was impaired. Thus, it is conceivable that the *swh/swh* rat will provide a good experimental model to clarify the mechanisms involved in the development of skin appendages, most of which are derived from ectoderm [20].

In our previously reported linkage analysis, *swh* mapped to the telomeric part of rat Chr 17. At that time, the physical location of the *swh* locus could not be accurately determined because a SSLP marker, *D17Rat140*, which defined the distal side of the *swh* locus was, in the earlier public rat genome linkage map, erroneously assigned to the middle part of Chr 17 and not to the telomeric part of Chr 17. Recently, with the development of more than 20,000 single nucleotide polymorphism (SNP) markers for 167 rat inbred strains and with the haplotype mapping data from the genotyping of these SNPs, the genome linkage map has been improved [21]. In the improved rat genome map, *D17Rat140* and its neighboring genes are correctly mapped to the telomeric part of rat Chr 17. Thus, in addition to the 24 candidate genes selected from our previous linkage analysis, we also considered these newly mapped genes to be candidates of *swh* [20].

In this study, to demonstrate the suitability of the *swh* rat as an HED model, we investigated the pathology of tissues and organs in which morphological abnormalities in HED are known to occur. Furthermore, we identified the causative mutation of the *swh* phenotype using a positional cloning approach, and found a missense mutation in the death domain of EDARADD, that might explain the inability of the mutant *Edaradd* gene to activate NF-κB. Our findings suggest that *swh* is a loss-of-function mutation of the rat *Edaradd* and support the *swh/swh* rat as an excellent animal model of HED that can be used to investigate the pathological basis of the disease and to develop new therapies.

Methods

Animals

ACI/NKyo, WTC/Kyo, and WTC-*swh*/Kyo rats were provided by the Japanese National BioResource Project for the Rat and kept in our animal facility for all experiments in this study. Animal care and experimental procedures were approved by the Animal Research Committee, Kyoto University, Japan, and were conducted according to the Regulation on Animal Experimentation at Kyoto University.

Histopathology

For light microscopy, the tongue, eyelid, ventral skin, footpad, and preputial gland were harvested from WTC-*swh/swh* and WTC rats at 8 weeks of age. Tissues were fixed in 10% neutral-buffered formalin, embedded in paraffin, and stained with hematoxylin and eosin (HE).

Sweat tests and whole mount staining of mammary glands

The sweat test was performed as described previously [12]. Briefly, the hind paws of rats anesthetized with sevoflurane were painted with a solution of 3% (wt/vol) iodine in ethanol. Once dry, the paws were painted with a suspension of 40% (wt/vol) starch I mineral oil. Photographs were taken 1 min later and sweat was detected as dark spots. Mammary glands were prepared as a whole mount and stained as described previously [22].

Fine mapping of swh

For fine mapping of *swh*, F2 animals (n = 769) were produced by intercrossing (ACI/NKyo × WTC-*swh*) F1 rats. Homozygous *swh/swh* animals were identified at 3-4 weeks of age based on the appearance of the sparse-and-waved hair phenotype. One hundred and ninety-eight *swh/swh* homozygotes were used for fine mapping of *swh*. Genomic DNA was prepared from tail biopsies using the automatic DNA purification system (PI-200; Kurabo, Japan).

RNA extraction, RT-PCR and direct sequencing

Total RNA was extracted from the skin of 2-week-old animals. RNA preparation, RT-PCR and direct sequencing of PCR products were performed as described

previously [23]. Rat *Edaradd* cDNAs were amplified with 6 sets of primers (Table 1). The PCR products overlapped each other and spanned the entire coding sequence of *Edaradd*.

Transient transfection and reporter assays

The NF-κB assay was designed to test for activation of the NF-κB responsive promoter. HEK293T cells grown in poly-L-lysine coated 24-well plates were transfected using SuperFect (Qiagen) with 1.2 μg pNF-κB-Luc (Clontech), 2 μg pRL-TK, and an increasing amount of expression vectors encoding the wild-type EDARADD or the *swh*-type EDARADD (Pro153Ser). The Luc reporter of the pNF-κB-Luc encodes firefly luciferase. The HSV-TK (herpes simplex virus thymidine kinase) promoter drives renilla luciferase in pRL-TK. Total DNA was adjusted to 2.6 μg by adding pCMV-HA (Clontech) vector as necessary. Luciferase activity was measured using the Dual-Luciferase Reporter Assay System (Promega) 48 h after transfection, according to the manufacturer's protocol.

Results

Phenotypes of *swh/swh* rat as hypohidrotic ectodermal dysplasia (HED)

Patients with HED display defective development of hair, teeth, sweat glands, and several exocrine glands, such as sebaceous, salivary, meibomian, and lacrimal [1,24]. To evaluate the relevance of the *swh/swh* rat as a HED model, we looked for developmental defects in those tissues of *swh/swh* rats. In addition to defects of the hair, skin, and mammary glands, which have been reported previously [20] (Figure 1A, B), we found defects in the sweat, meibomian, preputial, and tongue glands. In these tissues, the exocrine glands were absent in the *swh/swh* rats (Figure 1C, D, E, F). In the sweat test, no sweat was detected in *swh/swh* rats, indicating that the sweat glands were functionally defective (Figure 1C). We also found a reduced number of cusps in the lower first molars in the *swh/swh* rats (Figure 1G).

In the Eda pathway mutant mice, *Tabby, downless,* and *crinkled,* a kinked tail tip, a bald patch behind the ear, and abnormal pelage hair composition are characteristic. Similarly, in *swh/swh* rat, the pelage hair was composed of only an abnormal awl hair (Figure 1A); however, the tail had hair on it, the frequency of kinked tail was low, and the bald patch behind the ear was not found (Figure 1G).

These findings indicate that the mutant phenotypes of *swh/swh* rats are similar to developmental defects in HED patients and in the established mouse models; therefore, it is likely that the *swh/swh* rat will be suitable as a model of HED.

Positional cloning of *swh*

In a previous study, we mapped *swh* to rat Chr 17 [20]. To more specifically map the position of the *swh* locus, we genotyped F2 intercross progeny for markers known to be closely linked to *swh*. There was only one recombinant chromosome between *swh* and either *D17Rat132* or *D17Rat140* in 396 meioses (= 198 × 2) and we were able to map *swh* to the most distal part of Chr17 (Figure 2A). The rat genome map (RGSC v3.4) showed two genes in the *swh* locus, *Ero1lb* (ERO1-like beta (*S. cerevisiae*)) and *Edaradd* (ectodysplasin-A receptor-associated death domain). The mouse mutant of *Edaradd* is called *crinkled* (*cr*) and mice that carry this mutation show a sparse hair phenotype that is similar to that of the *swh* rat [25]. Additionally, mutations in the human *EDARADD* gene have been found in families affected with HED [6,26]. Thus, we considered *Edaradd* as a good candidate of *swh*. Although the abnormal expression of *Edaradd* mRNA was not detected in the skin of *swh/swh* rats (data not shown), we found a missense mutation (C to T) in exon 6 of the *swh/swh Edaradd* gene. This mutation was deduced to change proline to serine at the 153rd amino acid (Pro153Ser) of the rat EDARADD protein (Figure 2B). The 153rd amino acid is located in the death domain of EDARADD and is highly conserved in vertebrates (Figure 2C). These findings suggest that the Pro153Ser missense mutation of the *Edaradd* gene is causative of the phenotypes of *swh/swh* rats.

Reporter assay for the Pro153Ser mutant EDARADD

Overexpression of *Edaradd* in 293T cells activates NF-κB in a dose-dependent manner [25]. To examine whether Pro153Ser *Edaradd* can activate NF-κB, we carried out a reporter assay. As shown in Figure 3, wild-type *Edaradd*

Table 1 PCR primers used to amplify rat *Edaradd* cDNA

Primer set	Forward (5′ > 3′)	Reverse (5′ > 3′)
Edaradd-1&2	CTGAGAGAGAGTCGCGCATT	GCCACAGCTGTTCCCATAG
Edaradd-3&4	GCCCAGAAAAGGCAGCTC	GGAAAACCTTTGGAGTTTCTGA
Edaradd-5&6	CGATGAGCCAGCTTTACCTC	GGATAATTGGGTAACTATTCTCAACC
Edaradd-7&8	TCCATCCCAATTTTACCAACA	CGGCAAGCATTTTAATGACC
Edaradd-9&10	CAGTCAGCCCCTTGCACT	GCATGCTCTCATCAACATGG
Edaradd-11&12	TGTCACCAATGTGGTAGAAAAA	CAGGGATAACCACTGCCTGT

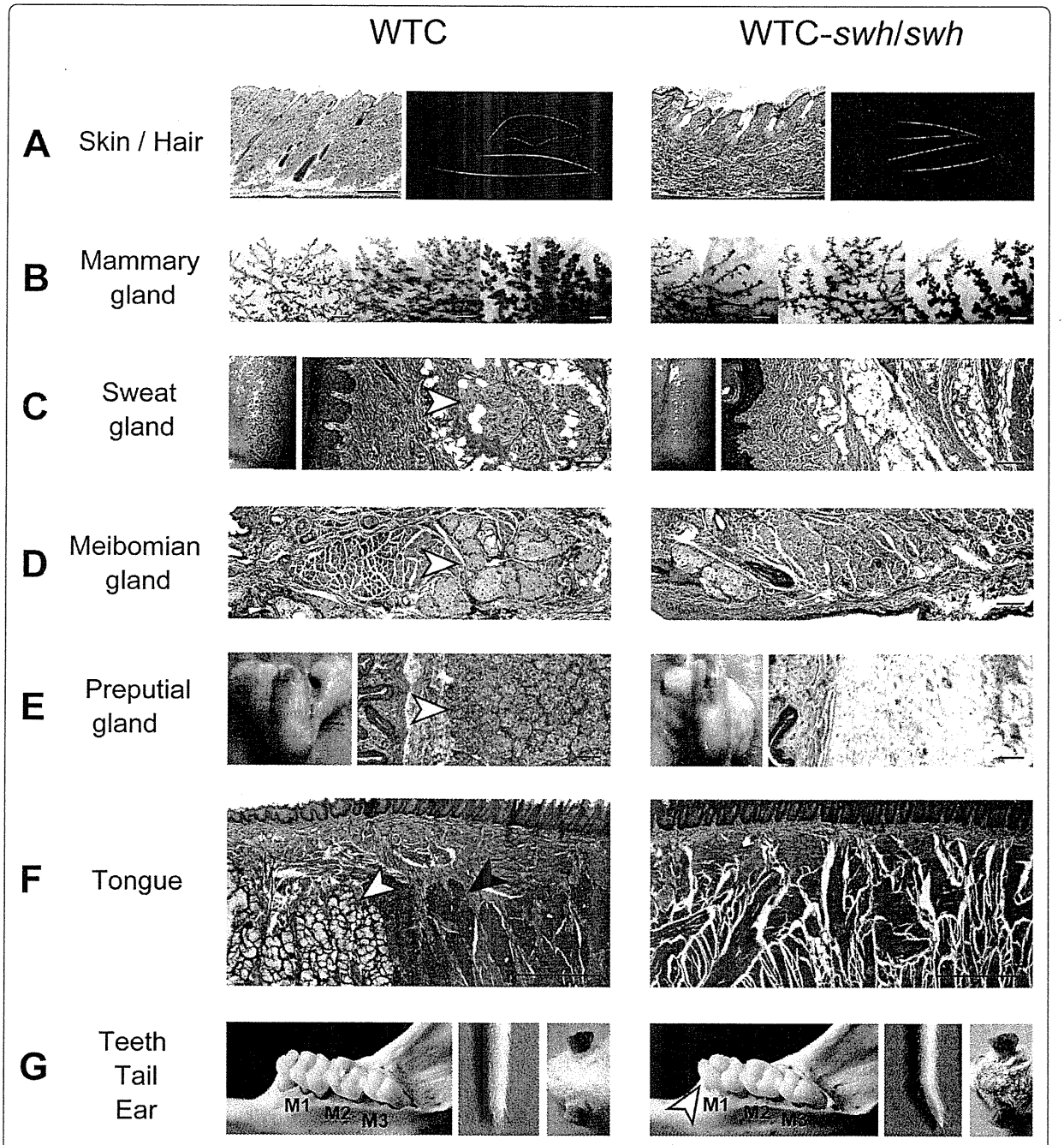

Figure 1 Phenotypes of the swh/swh rat as hypohidrotic ectodermal dysplasia (HED). A, Sections of the dorsal skin (left) and hair (right). Incomplete hair follicles are evident in *swh/swh* rat. Scale bar, 0.5 mm. The WTC rat has four hair types; auchene, zigzag, awl and guard, while the *swh/swh* rat have only the abnormal awl hair. B, Whole mount stained mammary glands; 6-week-old (left), 8-week-old (center), and pregnant day 9 (right). Mammary gland branching is poor in *swh/swh* rat. Scale bar, 1 mm. C, Sweat test results (left) and section of the footpads. Sweat, detected as dark spots, is not seen in *swh/swh* rat. Sweat glands (arrowhead) are present in WTC rat and absent in *swh/swh* rat. Scale bar, 100 μm. D, Sections of the eyelid. The meibomian glands (arrowhead) are present in WTC rat and absent in *swh/swh* rat. Scale bar, 100 μm. E, An entire view (left) and a section of the preputial gland (right). The preputial gland is atrophied in male *swh/swh* rat. Acinous glands (arrowhead) are present in WTC rat and absent in *swh/swh* rat. Scale bar, 100 μm. F, Section of the tongue. Both mucous (open arrowhead) and serous (filled arrowhead) glands are present in WTC rat and neither is seen in *swh/swh* rat. Scale bar, 0.5 mm. **G**, Buccal views of lower molars (left), tip of tail (center), and posterior auricular region (right). Cusp number is reduced in the first molar (arrow head) in *swh/swh* rat. Some *swh/swh* rats show the kink tail. The bald patch behind the ear was not evident in the *swh/swh* rat.

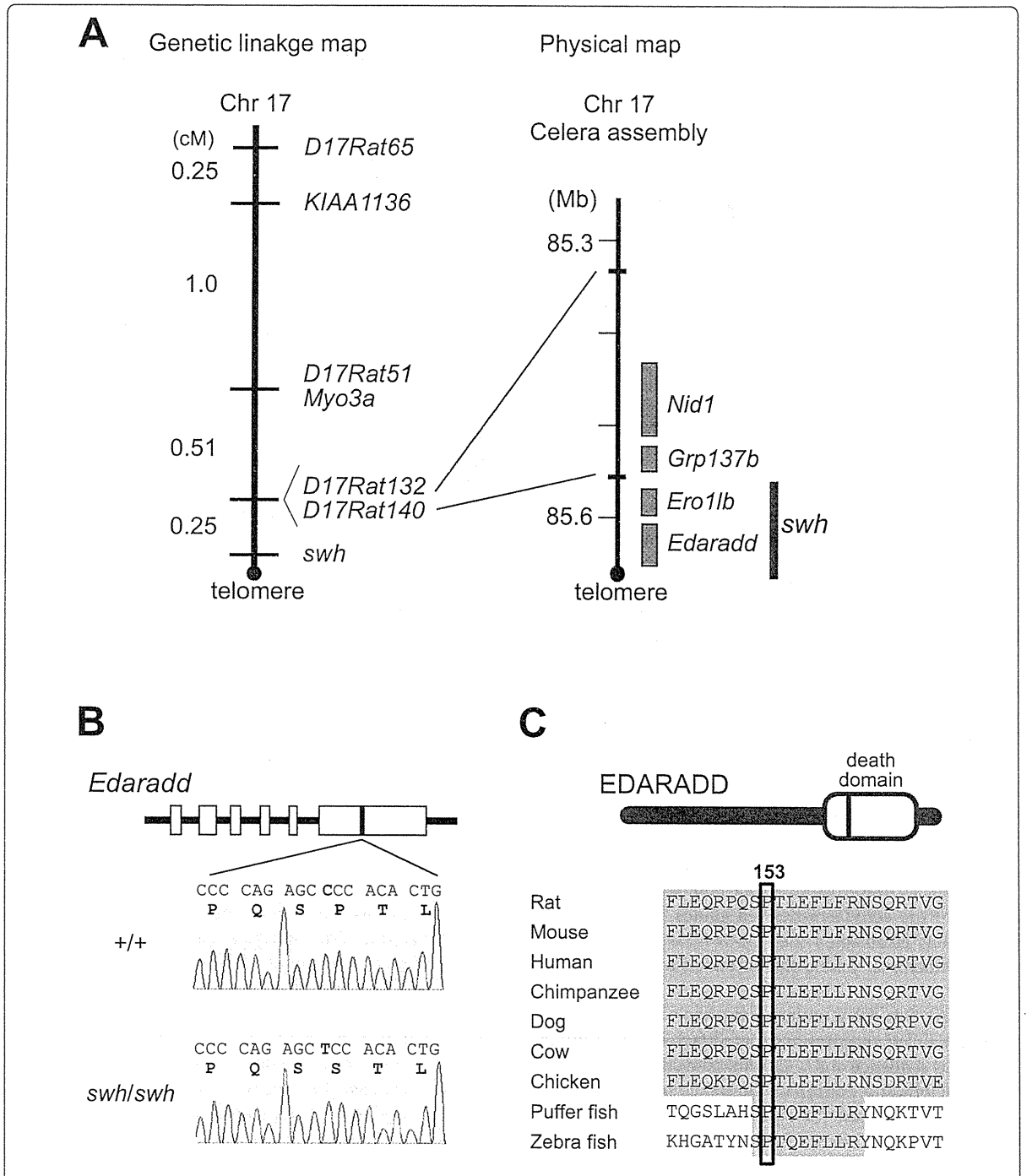

Figure 2 Identification of the rat *swh* mutation. A, Fine mapping of *swh* (left) and physical mapping of *swh* (right). The *swh* genetically mapped to the most telomeric part of rat Chr17, 0.25-cM distal from *D17Rat132* and *D17Rat140*. In the physical map, the *swh* locus is localized to a ~0.2-Mb region between *D17Rat140* and the telomere. Both *Ero1lb* and *Edaradd* have been mapped within the *swh* locus. B, Sequence analysis of *Edaradd* gene of wild-type and *swh/swh* rats. In the genomic DNA of *swh/swh* rat, a C to T (red) transition is present in exon 6 of rat *Edaradd* gene. This changes proline to serine at codon 153 of the deduced EDARADD protein. Rat codon 153 corresponds to codon 156 of mouse EDARADD isoform 1 (NP_598398) and codon 153 human EDARADD isoform B (NP_542776). C, Amino-acid sequence alignment of a region of the EDARADD death domain from different species. The 153rd amino acid that is altered in *swh/swh* rat is highly conserved in the vertebrates.

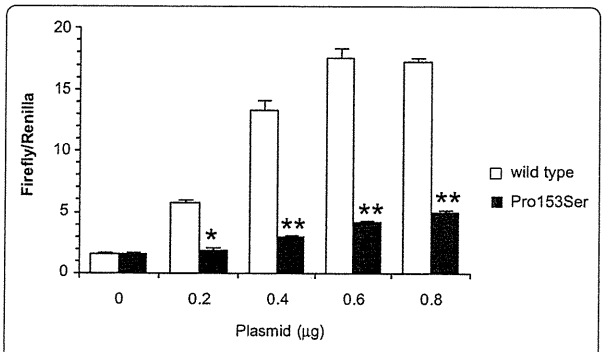

Figure 3 Loss of NF-κB activation by the Pro153Ser Edaradd mutant protein. 293T cells were transfected with 1.2 μg pNF-κB-luciferase reporter gene plasmid, 2 μg pRL-TK, and the amounts of each expression construct were measured in a reporter assay. The expression levels of luciferase were normalized to those of the internal control. Relative NF-κB activity in wild-type transfected cells increased in a dose-dependent manner, while significantly lower relative NF-κB activity was observed in the Pro153Ser *Edaradd*-transfected cells. *P < 0.01, **P < 0.001.

activated NF-κB in a dose-dependent manner. Meanwhile, Pro153Ser *Edaradd* showed significantly lower transcriptional activity of NF-κB than the wild type. The expression level of the Pro153Ser EDARADD protein detected by western blotting was not different from that of the wild type (data not shown). These findings indicate that the Pro153Ser missense mutation of the rat *Edaradd* gene could not activate NF-κB and that the Eda signaling pathway failed to function in *swh/swh* rats.

Discussion

In this study, we demonstrated that the *swh/swh* rat harbored a Pro153Ser mutation in the *Edaradd* gene and showed typical symptoms of HED, such as sparse hair, oligodontia, inability to sweat, and developmental defects of the ectoderm-derived glands [27]. Hence, we successfully established the *swh/swh* rat as a genetically and phenotypically well-characterized disease model of HED.

EDARADD is a 208 amino acid protein consisting of an N-terminal Tnf receptor-associated factor (Traf)-binding consensus sequence and a C-terminal death domain (DD). The Traf-binding consensus sequence of EDARADD is used as a docking site for Traf1, Traf2, and Traf3, thereby recruiting Traf members and leading eventually to the activation of NF-κB [6]. The DD is involved in self-association of EDARADD and its interaction with EDAR [6,25]. Thus, EDARADD is central to Edar signaling. The N-terminal region is responsible for signal transduction and the C-terminal DD is required for receptor engagement.

To date, four *EDARADD* mutations have been found in a subset of human HED, one leads to autosomal dominant inheritance (Leu112Arg) [26], while the others lead to autosomal recessive inheritance (Glu142Lys, Pro121Ser, and Thr135-Val136del) [6,28,29]. All of these mutations are located in the DD and functional analyses showed that they resulted in the failure of EDARADD to interact with EDAR and to activate NF-κB. In the *crinkled* mouse, a genomic region of ~66-kb or more which includes exon 6 that encodes the entire DD, is deleted [25]. The *crinkled* mouse displays developmental defects in hair follicles, teeth, and sweat glands [30,31]. Hence, it is possible that a mutation in the DD of EDARADD is necessary for the HED syndrome to be manifested both in human and mouse.

All members of the DD superfamily form a highly compact structure comprising six antiparallel α-helix that is involved in homotypic and heterotypic protein-protein complex formation [32]. The region spanning the α1 to α4 helices of the DD of MyD88, a member of the death receptor superfamily, is required for its interaction with a downstream kinase [33]. A comparison of the amino acid sequences of the DD superfamily revealed that the Pro153-Ser missense mutation found in the present study is located in the α4 helix of the DD of EDARADD. This mutation may cause a profound change in the polarity of a crucial region and eventually diminish NF-κB signaling. It is likely that Pro153Ser affects the structure of the DD thereby interfering in the interaction of EDARADD with EDAR.

Mutations affecting the Eda pathway are known in medaka [13], zebrafish [14], mouse [4,6,8], cattle [15-18], dog [19], and human [3,5,6]. Of them, the mouse mutants have been widely characterized as a model organism of HED. Here we report the *swh* mutation as the first example of a mutation in the Eda pathway in the rat.

Because the rat is closely related to the mouse, it is important to recognize how the rat *Edaradd* mutant phenotype matches the mouse Eda pathway mutant phenotypes. Similar to the mouse mutants, the *swh/swh* rat displayed sparse hair, misshapen teeth, and absence of sweating. Additionally, like the Eda pathway mutant, the *swh/swh* rat had only abnormal awl hair in the coat. The *swh/swh* rat showed a lack of the ectoderm-derived glands, meibomian, preputial, and tongue. Interestingly, both serous and mucous glands were absent in the tongue of the *swh/swh* rat. This is a clear difference from the mouse Eda pathway mutants that lacked mucous glands but had serous glands in the tongue [34]. Moreover, in contrast to the complete absence of tail hair in the Eda pathway mutant mice, the *swh/swh* rat had hair on its tail. The penetrance of the kink tail phenotype was low in the *swh/swh* rat, while almost all Eda pathway mutant mice showed the kink tail. Lastly, the bald patch behind the ear was not present in the *swh/swh* rat, although it was a very characteristic phenotype of the Eda pathway mutant mice.

Why these phenotypes are different between the Eda pathway mutant mice and the *swh/swh* rats is yet to be explained. However, different types of mutations could possibly explain the differences. The mouse *crinkled* mutation is a deletion [6], while the *swh* mutation is missense. Although the Luc-reporter assay strongly suggested that *swh* is a null mutation, the possibility that *swh* might be a hypomorphic mutation cannot be eliminated because the activation of NF-κB found in the assay was very low. In the Eda pathway mutant mice, the mammary, salivary and tracheal submucosal glands have been well characterized [9,10]. Further analyses of these glands in *swh/swh* rats will give further insights into the functions of the Eda pathway genes in the development of these glands.

Conclusions

We successfully established the *swh/swh* rat as the first rat model of HED and identified *swh* as a Pro135Ser missense mutation in the *Edaradd* gene. The Pro135Ser mutant protein failed to activate NF-κB in the Eda signaling pathway. Thus, the *swh/swh* rat is a good model that can be used to investigate the pathological basis of HED.

Acknowledgements and Funding

The authors are grateful to the National BioResource Project for the Rat for providing the ACI/NKyo, WTC/Kyo, and WTC-*swh*/Kyo rat strains. This work was supported in part by the Grants-in-aid for Scientific Research from the Japan Society for the Promotion of Science (21300153 to TK) and by a Grant-in-aid for Cancer Research from the Ministry of Health, Labour and Welfare (to TK).

Authors' contributions

TK and MY performed the genetic and molecular biological experiments. RH and HH performed the histological examinations. TK wrote the paper and HH and TS revised the manuscript. All authors read and approved the final manuscript.

Received: 29 July 2011 Accepted: 21 October 2011
Published: 21 October 2011

References

1. Mikkola ML, Thesleff I: Ectodysplasin signaling in development. *Cytokine Growth Factor Rev* 2003, 14(3-4):211-224.
2. Salisbury DM, Stothers JK: Hypohidrotic ectodermal dysplasia and sudden infant death. *Lancet* 1981, 1(8212):153-154.
3. Kere J, Srivastava AK, Montonen O, Zonana J, Thomas N, Ferguson B, Munoz F, Morgan D, Clarke A, Baybayan P, *et al*: X-linked anhidrotic (hypohidrotic) ectodermal dysplasia is caused by mutation in a novel transmembrane protein. *Nat Genet* 1996, 13(4):409-416.
4. Srivastava AK, Pispa J, Hartung AJ, Du Y, Ezer S, Jenks T, Shimada T, Pekkanen M, Mikkola ML, Ko MS, *et al*: The Tabby phenotype is caused by mutation in a mouse homologue of the *EDA* gene that reveals novel mouse and human exons and encodes a protein (ectodysplasin-A) with collagenous domains. *Proc Natl Acad Sci USA* 1997, 94(24):13069-13074.
5. Monreal AW, Ferguson BM, Headon DJ, Street SL, Overbeek PA, Zonana J: Mutations in the human homologue of mouse dl cause autosomal recessive and dominant hypohidrotic ectodermal dysplasia. *Nat Genet* 1999, 22(4):366-369.
6. Headon DJ, Emmal SA, Ferguson BM, Tucker AS, Justice MJ, Sharpe PT, Zonana J, Overbeek PA: Gene defect in ectodermal dysplasia implicates a death domain adapter in development. *Nature* 2001, 414(6866):913-916.
7. Mikkola ML: Molecular aspects of hypohidrotic ectodermal dysplasia. *Am J Med Genet A* 2009, 149A(9):2031-2036.
8. Headon DJ, Overbeek PA: Involvement of a novel Tnf receptor homologue in hair follicle induction. *Nat Genet* 1999, 22(4):370-374.
9. Chang SH, Jobling S, Brennan K, Headon DJ: Enhanced Edar signalling has pleiotropic effects on craniofacial and cutaneous glands. *PLoS One* 2009, 4(10):e7591.
10. Melnick M, Phair RD, Lapidot SA, Jaskoll T: Salivary gland branching morphogenesis: a quantitative systems analysis of the Eda/Edar/NFκB paradigm. *BMC Dev Biol* 2009, 9:32.
11. Gruneberg H: The glandular aspects of the tabby syndrome in the mouse. *J Embryol Exp Morphol* 1971, 25(1):1-19.
12. Gaide O, Schneider P: Permanent correction of an inherited ectodermal dysplasia with recombinant EDA. *Nat Med* 2003, 9(5):614-618.
13. Kondo S, Kuwahara Y, Kondo M, Naruse K, Mitani H, Wakamatsu Y, Ozato K, Asakawa S, Shimizu N, Shima A: The medaka *rs-3* locus required for scale development encodes ectodysplasin-A receptor. *Curr Biol* 2001, 11(15):1202-1206.
14. Harris MP, Rohner N, Schwarz H, Perathoner S, Konstantinidis P, Nusslein-Volhard C: Zebrafish eda and edar mutants reveal conserved and ancestral roles of ectodysplasin signaling in vertebrates. *PLoS Genet* 2008, 4(10):e1000206.
15. Drogemuller C, Distl O, Leeb T: Partial deletion of the bovine *ED1* gene causes anhidrotic ectodermal dysplasia in cattle. *Genome Res* 2001, 11(10):1699-1705.
16. Drogemuller C, Peters M, Pohlenz J, Distl O, Leeb T: A single point mutation within the *ED1* gene disrupts correct splicing at two different splice sites and leads to anhidrotic ectodermal dysplasia in cattle. *J Mol Med (Berl)* 2002, 80(5):319-323.
17. Ogino A, Kohama N, Ishikawa S, Tomita K, Nonaka S, Shimizu K, Tanabe Y, Okawa H, Morita M: A novel mutation of the bovine *EDA* gene associated with anhidrotic ectodermal dysplasia in Holstein cattle. *Hereditas* 2011, 148(1):46-49.
18. Gargani M, Valentini A, Pariset L: A novel point mutation within the *EDA* gene causes an exon dropping in mature RNA in Holstein Friesian cattle breed affected by X-linked anhidrotic ectodermal dysplasia. *BMC Vet Res* 2011, 7:35.
19. Casal ML, Scheidt JL, Rhodes JL, Henthorn PS, Werner P: Mutation identification in a canine model of X-linked ectodermal dysplasia. *Mamm Genome* 2005, 16(7):524-531.
20. Kuramoto T, Morimura K, Nomoto T, Namiki C, Hamada S, Fukushima S, Sugimura T, Serikawa T, Ushijima T: Sparse and wavy hair: a new model for hypoplasia of hair follicle and mammary glands on rat chromosome 17. *J Hered* 2005, 96(4):339-345.
21. Saar K, Beck A, Bihoreau MT, Birney E, Brocklebank D, Chen Y, Cuppen E, Demonchy S, Dopazo J, Flicek P, *et al*: SNP and haplotype mapping for genetic analysis in the rat. *Nat Genet* 2008, 40(5):560-566.
22. Rothschild TC, Boylan ES, Calhoon RE, Vonderhaar BK: Transplacental effects of diethylstilbestrol on mammary development and tumorigenesis in female ACI rats. *Cancer Res* 1987, 47(16):4508-4516.
23. Kuramoto T, Kuwamura M, Tokuda S, Izawa T, Nakane Y, Kitada K, Akao M, Guenet JL, Serikawa T: A mutation in the gene encoding mitochondrial Mg^{2+} channel MRS2 results in demyelination in the rat. *PLoS Genet* 2011, 7(1):e1001262.
24. Reed WB, Lopez DA, Landing B: Clinical spectrum of anhidrotic ectodermal dysplasia. *Arch Dermatol* 1970, 102(2):134-143.
25. Yan M, Zhang Z, Brady JR, Schilbach S, Fairbrother WJ, Dixit VM: Identification of a novel death domain-containing adaptor molecule for ectodysplasin-A receptor that is mutated in crinkled mice. *Curr Biol* 2002, 12(5):409-413.
26. Bal E, Baala L, Cluzeau C, El Kerch F, Ouldim K, Hadj-Rabia S, Bodemer C, Munnich A, Courtois G, Sefiani A, *et al*: Autosomal dominant anhidrotic ectodermal dysplasias at the EDARADD locus. *Hum Mutat* 2007, 28(7):703-709.
27. Pispa J, Thesleff I: Mechanisms of ectodermal organogenesis. *Dev Biol* 2003, 262(2):195-205.
28. Chassaing N, Cluzeau C, Bal E, Guigue P, Vincent MC, Viot G, Ginisty D, Munnich A, Smahi A, Calvas P: Mutations in *EDARADD* account for a small proportion of hypohidrotic ectodermal dysplasia cases. *Br J Dermatol* 2010, 162(5):1044-1048.
29. Suda N, Bazar A, Bold O, Jigjid B, Garidkhuu A, Ganburged G, Moriyama K: A Mongolian patient with hypohidrotic ectodermal dysplasia with a novel P121S variant in *EDARADD*. *Orthod Craniofac Res* 2010, 13(2):114-117.

30. Kindred B: **The expression of the Tabby and crinkled genes in different genetic backgrounds in the mouse.** *Genetics* 1967, **55(1)**:173-178.
31. Rao MS, Jaszczak E, Landis SC: **Innervation of footpads of normal and mutant mice lacking sweat glands.** *J Comp Neurol* 1994, **346(4)**:613-625.
32. Weber CH, Vincenz C: **The death domain superfamily: a tale of two interfaces?** *Trends Biochem Sci* 2001, **26(8)**:475-481.
33. Loiarro M, Gallo G, Fanto N, De Santis R, Carminati P, Ruggiero V, Sette C: **Identification of critical residues of the MyD88 death domain involved in the recruitment of downstream kinases.** *J Biol Chem* 2009, **284(41)**:28093-28103.
34. Wells KL, Mou C, Headon DJ, Tucker AS: **Defects and rescue of the minor salivary glands in Eda pathway mutants.** *Dev Biol* 2011, **349(2)**:137-146.

doi:10.1186/1471-2156-12-91
Cite this article as: Kuramoto *et al.*: A rat model of hypohidrotic ectodermal dysplasia carries a missense mutation in the *Edaradd* gene. *BMC Genetics* 2011 12:91.

DNA Repair 11 (2012) 259–266

Contents lists available at SciVerse ScienceDirect

DNA Repair

journal homepage: www.elsevier.com/locate/dnarepair

Activation of AMP-activated protein kinase by MAPO1 and FLCN induces apoptosis triggered by alkylated base mismatch in DNA

Teik How Lim[a], Ryosuke Fujikane[b], Shiori Sano[b,c], Ryuji Sakagami[c], Yoshimichi Nakatsu[a], Teruhisa Tsuzuki[a], Mutsuo Sekiguchi[d], Masumi Hidaka[b,*]

[a] Department of Medical Biophysics and Radiation Biology, Faculty of Medical Sciences, Kyushu University, Fukuoka 812-8582, Japan
[b] Department of Physiological Science and Molecular Biology, Fukuoka Dental College, Fukuoka 814-0193, Japan
[c] Department of Odontology, Fukuoka Dental College, Fukuoka 814-0193, Japan
[d] Frontier Research Center, Fukuoka Dental College, Fukuoka 814-0193, Japan

ARTICLE INFO

Article history:
Received 31 August 2011
Received in revised form 9 November 2011
Accepted 28 November 2011
Available online 29 December 2011

Keywords:
AMPK
Apoptosis
Folliculin/BHD
MAPO1/FNIP2/FNIPL
O^6-methylguanine

ABSTRACT

O^6-Methylguanine produced in DNA by the action of simple alkylating agents, such as *N*-methyl-*N*-nitrosourea (MNU), causes base-mispairing during DNA replication, thus leading to mutations and cancer. To prevent such outcomes, the cells carrying O^6-methylguanine undergo apoptosis in a mismatch repair protein-dependent manner. We previously identified MAPO1 as one of the components required for the induction of apoptosis triggered by O^6-methylguanine. MAPO1, also known as FNIP2 and FNIPL, forms a complex with AMP-activated protein kinase (AMPK) and folliculin (FLCN), which is encoded by the *BHD* tumor suppressor gene. We describe here the involvement of the AMPK–MAPO1–FLCN complex in the signaling pathway of apoptosis induced by O^6-methylguanine. By the introduction of siRNAs specific for these genes, the transition of cells to a population with sub-G_1 DNA content following MNU treatment was significantly suppressed. After MNU exposure, phosphorylation of AMPKα occurred in an MLH1-dependent manner, and this activation of AMPK was not observed in cells in which the expression of either the *Mapo1* or the *Flcn* gene was downregulated. When cells were treated with AICA-ribose (AICAR), a specific activator of AMPK, activation of AMPK was also observed in a MAPO1- and FLCN-dependent manner, thus leading to cell death which was accompanied by the depolarization of the mitochondrial membrane, a hallmark of the apoptosis induction. It is therefore likely that MAPO1, in its association with FLCN, may regulate the activation of AMPK to control the induction of apoptosis triggered by O^6-methylguanine.

1. Introduction

Most of the DNA lesions produced by internal and external agents can be removed by cellular DNA repair enzymes, while cells with un-repaired lesions are eliminated by apoptosis. The biological significance of these two mechanisms is clearly shown when organisms lacking one or both of these cellular functions are exposed to simple alkylating agents, such as *N*-methyl-*N*-nitrosourea (MNU) and *N*-methyl-*N'*-nitro-*N*-nitrosoguanidine (MNNG), which alkylate purine and pyrimidine bases in DNA [1]. Among the various modified bases thus produced, O^6-methylguanine is of particular importance since this modified base can pair with thymine as well as cytosine during DNA replication, leading to induction of mutation and cancer [2,3]. Organisms possess a specific DNA repair enzyme, O^6-methylguanine–DNA methyltransferase (MGMT), which transfers a methyl-group from O^6-methylguanine in DNA onto the enzyme molecule, thereby repairing the DNA lesion in a single step reaction [4,5]. When the modified base is not repaired, an O^6-methylguanine–thymine pair is formed through DNA replication and this mismatch can be recognized by a mismatch repair protein complex, composed of MSH2, MSH6, MLH1 and PMS2, which induces apoptosis to exclude cells carrying the mutation-evoking DNA lesions [6–8]. It is noteworthy that *Mgmt*$^{-/-}$ mice, which lack the DNA repair enzyme specific for O^6-methylguanine, are hypersensitive to both the killing and to the tumorigenic action of alkylating chemicals [9–12] and these dual effects can be dissociated by the introduction of an additional defect in mismatch repair genes. Mice with mutations in both alleles of the *Mgmt* and the *Mlh1* genes, the latter encoding a protein involved in the recognition of mismatched base, are as resistant to MNU as are wild-type mice in terms of survival, but are much more susceptible to MNU-induced tumorigenesis than wild-type mice

* Corresponding author at: Department of Physiological Science and Molecular Biology, Fukuoka Dental College, 2-15-1 Tamura, Sawara-ku, Fukuoka 814-0193, Japan. Tel.: +81 92 801 0411x310; fax: +81 92 801 0685.
E-mail address: hidaka@college.fdcnet.ac.jp (M. Hidaka).

1568-7864/$ – see front matter © 2011 Elsevier B.V. All rights reserved.
doi:10.1016/j.dnarep.2011.11.006